Naval Research Laboratory

Washington, DC 20375-5000

NRL Memorandum Report 6627

Relativistic Klystron Amplifiers Driven by Modulated Intense Relativistic Electron Beams

Y. Y. Lau, M. Friedman, J. Krall, and V. Serlin

Beam Physics Branch
Plasma Physics Division

April 11, 1990

REPORT DOCUMENTATION PAGE

Form Approved
OMB No. 0704-0188

1. AGENCY USE ONLY (Leave blank)	2. REPORT DATE	3. REPORT TYPE AND DATES COVERED
	1990 April 11	Interim

4. TITLE AND SUBTITLE

Relativistic Klystron Amplifiers Driven by Modulated Intense Relativistic Electron Beams

5. FUNDING NUMBERS

DOE=47-2757
Contract # AI05-86-ER13585
SDI/IST=47-2915

6. AUTHOR(S)

Y. Y. Lau, M. Friedman, J. Krall, and V. Serlin

7. PERFORMING ORGANIZATION NAME(S) AND ADDRESS(ES)

Naval Research Laboratory
Washington, DC 20375-5000

8. PERFORMING ORGANIZATION REPORT NUMBER

NRL Memorandum Report 6627

9. SPONSORING/MONITORING AGENCY NAME(S) AND ADDRESS(ES)

DOE
Washington, DC 20545

SDIO/IST
Harry Diamond Laboratory
Adelphi, MD 20783

10. SPONSORING/MONITORING AGENCY REPORT NUMBER

11. SUPPLEMENTARY NOTES

12a. DISTRIBUTION/AVAILABILITY STATEMENT

Approved for public release;
distribution unlimited.

12b. DISTRIBUTION CODE

13. ABSTRACT (Maximum 200 words)

In this paper, we give an overview of the novel relativistic klystron amplifiers which are currently under active study at the Naval Research Laboratory. These amplifiers are driven by an annular intense relativistic electron beam (500 kV, 10 kA range) which is modulated by an external rf source (1.3 GHz, 100 kW range). Experiments, theory, simulation and simple models are presented to illustrate the unusual properties of such devices, which result from the intense space charge of the beam. Chief among them include electrostatic insulation against vacuum breakdown at high power levels, efficient current modulation, short bunching length, and amplitude and phase stability of the output signal. Many of these unexpected features were revealed in two separate experiments: one with the lower current beam (5 kA, 2 cm beam radius), and the other one with a higher current beam (16 kA, 6.6 cm beam radius). Three gigatwatts or rf power at 1.3 GHz were generated with the large diameter beam at an efficiency of 35 percent with 37 dB gain. These experiments will be reviewed, along with a combination of particle simulation results and analytic models which facilitate the interpretation. We pay special attention to the unfamiliar features of these amplifiers, and shall address the critical issues which need to be solved before such amplifiers can fulfill their potential in a wide range of applications.

14. SUBJECT TERMS

High power microwaves
Relativistic klystron amplifiers
Intense beam modulation

15. NUMBER OF PAGES

77

16. PRICE CODE

17. SECURITY CLASSIFICATION OF REPORT	18. SECURITY CLASSIFICATION OF THIS PAGE	19. SECURITY CLASSIFICATION OF ABSTRACT	20. LIMITATION OF ABSTRACT
UNCLASSIFIED	UNCLASSIFIED	UNCLASSIFIED	SAR

CONTENTS

RELATIVISTIC KLYSTRON AMPLIFIERS DRIVEN BY MODULATED INTENSE RELATIVISTIC ELECTRON BEAMS

I. Introduction

There is considerable current interest in relativistic klystron amplifiers (RKA) in the 1-20 GHz range with power requirement exceeding 10^8 watts. This interest arose from the pressing need of the accelerator community to look for a suitable rf source for high gradient acceleration [1]-[3] and from directed energy applications [4]. The inherent phase and amplitude stability of the RKA, and to a lesser extent the extensive experience with conventional klystrons [5], has made the RKA highly competitive relative to other high power microwave devices, such as the relativistic magnetron [6], [7], vircator [8], gyrotron [9], backward wave oscillator [10], etc., all of which have demonstrated capabilities in the generation of high power radiation in the above frequency range. High power cross field amplifiers have also been recently considered as a candidate of accelerator drivers [11].

At present, there are two lines of RKA research, with rather different characteristics. The first, which is the dominant approach, is represented by a consorted effort of accelerator builders [12]-[15], whose design philosophy parallels the conventional klystron, but with the beam energy being extended to the relativistic range (~ MeV) and current reaching ~ 1 kA. These RKA configurations are similar to conventional klystrons in their use of pencil beams and multiple gain cavities. They are also similar to the conventional klystrons in that the DC space charge of the beam is unimportant to their operation. RKA experiments of this type have recently produced 290 MW of rf power at 11.4 GHz [15]. The most serious problem, which has received considerable attention, lies with vacuum breakdown [12] at high power levels. This leads to the shortening of the pulse length in the output rf and has prompted several proposed cures, such

Manuscript approved February 14, 1990.

as the use of iron rings around the input cavities to shunt the magnetic field from the center, and the inclusion at the output gap of a traveling wave structure to reduce the electric stress [12], [15]. Compared with the aforementioned high power microwave devices, this line of RKA research is at a relatively advanced stage.

The other line of RKA research has been pursued mainly at the Naval Research Laboratory [16]-[18] which, thus far, involved significantly less effort. This work evolved from a series of experiments on intense beam modulation performed over the past ten years [19]-[21]. The geometry and the beam parameters are markedly different from those given in the preceding paragraphs: an annular intense relativistic electron beam [IREB] in the 500 kV, 10 kA range was generated from a field immersed, cold cathode and coaxial cavities were used to modulate the beam. Recently, single pulses of 3 GW coherent peak rf power at 1.3 GHz were generated in such an RKA, at an efficiency of 35% and pulse length ~ 120 ns [18]. The most remarkable feature of this configuration is the apparent lack of rf breakdown that is commonly taken to be inevitable at these high power levels. This unusual property is one of several that are the necessary result of the intense DC space charge of the high current beam and the specific geometries used. These phenomena will be discussed in this review. Since this is a relatively new subject, and is currently perceived as possessing great potential, we should mention at the outset that our experiments to date have been restricted to single pulse operation at low frequencies (~ 1.3 GHz). Repetitive capability [22] and scaling to higher frequencies ($\geq$ 10 GHz) are outstanding issues.

In this paper, we shall mainly concentrate on the unique properties associated with RKAs driven by modulated intense relativistic electron

beams. In Section II, we give a qualitative description of these RKA configurations. There, we shall give intuitive arguments to show that the DC space charge of the beam provides electrostatic insulation against rf breakdown, and to demonstrate that DC space charge effects may have assisted in the generation of the fully modulated beam. The simple exposition given there emerged after considerable experimentation, analytic theory and numerical simulation [16]-[21], [23]-[27]. In Section III, we analyze various theoretical aspects of the RKA, through particle simulation and analytic modeling. This will facilitate the interpretation of the experiments, which will be described in Section IV. In Section IV, we shall first review the experimental results on the modulation of a small diameter beam. This will be followed with a discussion of the subsequent experimentation with a large diameter beam at a substantially higher current, from which a 3 GW peak pulse of rf radiation was extracted. Some outstanding issues will be discussed in Section V.

II. Qualitative Description

A. Geometry

A schematic drawing of the Naval Research Laboratory RKA is shown in Fig. 1. An annular electron beam of voltage V_b ~ 500 kV, current I_o ~ 5-20kA and pulse length τ_p ~ 120 ns is injected into a drift region from a field immersed diode. This beam is modulated by a coaxial cavity, which is driven by an external rf source at a frequency of 1.3 GHz with power in the 100 kW range. This external rf source produces a gap voltage, at the first cavity, of the order of 30 kV. This relatively low voltage produces a velocity modulation of the beam, which is converted downstream to a current modulation, typically $\lesssim$ 10%. This current modulation can be

substantially increased by a second cavity, which is undriven but is tuned to the same frequency as the first cavity. It was shown in experiments that this undriven cavity may fully modulate the beam over a short distance, and the resultant current modulation exhibits excellent phase and amplitude stability [16], [17]. The kinetic power of this highly modulated beam is then converted to radiation through an rf converter which consists of a gap, a coaxial line supported by a few radial rods (which also serve as the return path for the DC current), a tuning stub, and an output window [Fig. 1]. This geometry has recently yielded 3 GW peak rf power which was radiated into air at 1.3 GHz, with an efficiency of 35% and pulse length exceeding 120 ns [18].

The above brief description of the RKA revealed several unusual features which are not expected from conventional klystrons: efficient current bunching (short bunching length) and the absence of rf breakdown during the relatively long rf pulse. These will be explained in a qualitative manner below. Other equally important properties, such as the amplitude and phase stability of the rf signal observed in the experiments, are confirmed in particle simulations and will be postponed to the next Section.

B. Limiting Current

Because of the important role played by the DC space charge, the concept of limiting current [28]-[30] needs to be reviewed to understand the RKA performance. For an intense beam, the potential energy associated with the DC space charge is significant - of the same order of magnitude as the beam voltage. The beam's kinetic energy in the drift region would be lower than the injection energy. Neglecting the transverse motions, conservation of energy for a DC beam gives

$$\gamma_{inj} = \gamma_o + \frac{I_o}{I_s \beta_o}, \qquad (1)$$

where $(\gamma_{inj}-1)m_o c^2$ represents the injection energy of an electron from the diode, γ_o is the relativistic mass factor associated with the drift motion, $\beta_o = v_o/c \equiv (1-1/\gamma_o^2)^{1/2}$, and $I_o/I_s\beta_o$ represents the DC potential energy associated with the space charge. Here, I_s is the current scale which depends only on the geometry. For a thin annular electron beam of radius r_b inside a hollow drift tube of radius r_w,

$$I_s = 8.53 \text{ kA}/\ell n(r_w/r_b). \qquad (2)$$

It is clear that when I_o is sufficiently large, Eq. (1) cannot be satisfied and beam propagation stops. This occurs when $I_o > I_c$, where I_c is the limiting current, given by

$$I_c = I_s(\gamma_{inj}^{2/3} - 1)^{3/2}, \qquad (3)$$

which is easily derived from Eq. (1). Note that the critical value I_c depends only on the diode voltage (γ_{inj}) and on the geometry.

As an example, for a small diameter beam with E_{inj} = 425 KeV, I_o = 5 kA, r_b = 1.9 cm and r_w = 2.4 cm, we find I_s = 36 kA and I_c = 12.6 kA. Here, the kinetic energy $(\gamma_o - 1)m_o c^2$ is 340 keV and the potential energy is 85 keV, which is a significant fraction of the injection energy. By comparison, the potential energy in conventional klystrons (or other RKAs which use pencil beams [12]-[15]) is negligible.

To achieve ultra high rf power, a high current beam would be required [31]. In order that Eq. (1) remains satisfied at high values of I_o (at a given value of γ_{inj}), I_s must assume a large value. This can be done by increasing both r_b and r_w, so that $r_b/r_w \to 1$ [cf. Eq. (2)].

Increasing r_b would allow the beam to hold a large amount of current, and bringing r_w close to r_b would reduce the potential depression from the DC space charge. Thus, our ultra high power RKA experiments tend to use a large diameter beam.

Note that the current scale I_s in Eq. (2) is modified if the wall is perturbed, say, by a coaxial cavity. In this case, I_s is reduced. Furthermore, we shall always resort to Eq. (1) as a guide in our interpretation of the RKA data. For low frequency modulation, Eq. (1) is an approximate statement of energy conservation.

C. A Gate Effect and Enhanced Current Bunching in an Intense Beam

Operation close to the limiting current leads to an unusual property which is not shared with a classical klystron. That property is the experimentally observed substantial current modulation immediately beyond a modulating gap. If the modulating voltage at the gap is sufficiently large, the instantaneous beam current may exceed the limiting value during the retarding phase of the rf cycle. This leads to strong current modulation as the beam exits the gap. Extending the above model, we assume that an rf voltage $V_1 \sin \omega t$ is imposed across the gap. The instantaneous values v (speed), β and γ of an electron are then given by

$$\gamma_{inj} = \gamma + \frac{I_o}{I_s \beta} + \frac{|e| V_1 \sin \omega t}{m_o c^2} . \qquad (4)$$

It is easy to show that Eq. (4) does not admit a (real) solution for β and γ if $V_1 \sin \omega t > V_{th}$, where

$$V_{th} = \frac{m_o c^2}{|e|} \left\{ \gamma_{inj} - \left[1 + \left(\frac{I_o}{I_c} \right)^{2/3} \left(\gamma_{inj}^{2/3} - 1 \right) \right]^{3/2} \right\} . \qquad (5)$$

The current modulation at the gap exit is absent if $V_1 < V_{th}$, but rises rapidly once $V_1 > V_{th}$, and becomes insensitive to V_1 if the latter substantially exceeds V_{th} [Fig. 2]. These features are also reflected qualitatively in experiments and in simulations [cf., Fig. 9 below]. The amount of current modulation at the gap is estimated to be [23]

$$\left(\frac{I_1}{I_o}\right)_{exit} \simeq \frac{\omega}{\pi}\int_{\hat{t}-\pi}^{\hat{t}} dt \sin \omega t = \frac{2}{\pi}\left(1 - \frac{V_{th}^2}{V_1^2}\right)^{1/2}, \qquad (6)$$

where $\hat{t} = (1/\omega) \sin^{-1}(V_{th}/V_1)$.

Even for a low modulation voltage, the following simple physical argument may offer some insight into the manner in which the quasi-DC space charge of the intense beam may enhance the current modulation. As a reference, let us compare the ballistic bunching process in a weak beam, as shown in Fig. 3a. In Fig. 3a, we show a "snapshot" of two drifting electrons, A and B, with velocities v_A and v_B, and separated by a distance L. The velocity difference $(v_A - v_B)$ is assumed to have been provided earlier by a modulating gap. It is easy to show that electron A needs to travel an extra distance $D = v_A L/(v_A - v_B)$ to "catch up" with electron B. This distance D is a measure of the bunching length. In the case of an intense beam, both electron A and electron B are retarded by the space charge potential of the beam. We may qualitatively envision this retarding potential as an effective "gravity" and the electrons A, B are now drifting against this "gravity" on an inclined plane [Fig. 3b]. For the same initial velocities v_A and v_B, and the same separation L between A and B, electron A will travel a distance D′ to catch up with electron B. In general, $D' < D$ as a retarding force will always produce a larger

fractional change in the velocity of the slower electron relative to the faster one. [A slow bicycle (electron B) climbing up an inclined plane against gravity g is more easily stopped than a fast bicycle (electron A)]. Thus, the bunching length is shortened by the space charge of an intense beam for the same velocity modulation. We believe that the combination of the gate effect, and the mechanism illustrated in Fig. 3, are responsible for the efficient current modulation of the IREB over a short distance. These processes were quantified in Refs. [17], [24], where we estimated the degree of shortening in the bunching length, and also the distortion of the propagation characteristics of the nonlinear slow space charge waves. The gate effect was conjectured earlier [16], but it became evident as numerical simulations were performed [17], [23] (see Fig. 9 below, for example).

D. Electrostatic Insulation [26]

It is not difficult to see that DC space charge effects associated with an annular intense beam can provide electrostatic insulation, thereby preventing the rf breakdown across a gap that is normally expected in the generation of high power rf. A floating, negative potential barrier, which may reach hundreds of kV at the gap [Fig. 4], is produced by the beam's space charge. This potential barrier strongly discourages electron emission across the gap. If the annular beam is tightly bunched, the space charge of the beam will be even higher and the tendency toward electrostatic insulation will be stronger accordingly. Particle simulations demonstrating electrostatic insulation will be presented in Section III. This unusual property of electrostatic insulation was noted in a previous calculation of electrostatic potential contours at the gap

[27]. There is also evidence that electrostatic insulation is playing a role in the observed rf pulse length of the RKA, as described in Section IV below.

Inside the coaxial cavity, the modulating rf electric field is in the radial direction. There, the strong axial solenoidal magnetic field (~ 10 kG) is sufficient to prevent rf breakdown [Fig. 4].

The combination of an annular intense beam and a coaxial cavity provides a crucial difference relative to the conventional klystron configurations which use a low current pencil beam and a "pill-box like" cavity. First, in a conventional klystron, the DC space charge of the low current beam is insufficient for electrostatic insulation. Second, the axial magnetic field in a conventional klystron is roughly parallel to the rf electric field at the gaps, thereby encouraging rf breakdown. In fact, shunting the axial magnetic fields from the gap region has been shown to be essential in eliminating breakdown in RKAs that use conventional klystron geometries [15].

III. Theory and Simulation

In this section, we give a more quantitative analysis of the various processes in the RKA via analytic theories and particle simulation. They are essential to the understanding of the RKA experiments as they are markedly different from the conventional klystron. The topics treated in this section include current modulation in both the small signal regime [Subsection A] and in the highly nonlinear regime [Subsection B]. The phase and amplitude stability, and the bunching processes are evident in the simulation. Electrostatic insulation and magnetic insulation will be given next [Subsection C]. This is followed by an estimate of the limiting

current which can be transported across a gap that is subject to a biased gap voltage [Subsection D]. There, we shall also examine the various factors which might determine the operation efficiency.

A. Current Modulation in the Small Signal Regime

The interaction at the first gap can be modelled via a small signal theory as the gap voltage there is only a small fraction of the beam voltage. The voltage and current modulation beyond the first gap may then be considered as a superposition of the small signal fast and slow space charge waves, just as in the conventional klystron theory. The propagation constants $k_f(\omega)$ and $k_s(\omega)$ of these waves need to be modified for the IREB, however.

Let $V_{10}\exp(j\omega t)$ be the gap voltage imposed on the beam at $z = 0$. This gap voltage excites space charge waves along the drift tube. Associated with these space charge waves is a small signal current wave and voltage wave $[I_1(z), V_1(z)]\exp(i\omega t - i\bar{k}z)$ where $\bar{k} = (k_f + k_s)/2$ and $I_1(z)$ and $V_1(z)$ are the current and voltage modulation on the beam. For an annular beam very close to the walls of a circular drift tube, the wavenumbers $k_f(\omega)$ and $k_s(\omega)$ are obtained from the solution of the dispersion relation [32]:

$$(\omega - kv_o)^2 = \alpha(k^2c^2 - \omega^2), \tag{7}$$

which is a second degree polynomial in k. Here, $v_o = \beta_o c$ is the drift speed of the electrons, c is the speed of light, and

$$\alpha \equiv I_o/(I_s\gamma_o^3\beta_o) \tag{8}$$

is proportional to the beam current. Equation (7) was derived under the assumption $k(r_w - r_b) \ll 1$. Note that the space charge waves as described

by Eq. (7) are nondispersive, i.e., the phase speeds ω/k_f and ω/k_s are independent of frequency [33]. Thus, at least at the small signal level, current bunches are shape-preserving. This fact may have contributed to the experimentally-observed coherence of the current modulation [16]. Note also that the "plasma frequency reduction factor" which usually enters in klystron analysis [34] was set equal to unity [35]. The current modulation $I_1(z)$ and voltage modulation $V_1(z)$ resulting from the gap voltage V_{10} then reads [16], [17]

$$I_1(z) = -j\ (V_{10}/Z)\ \sin\ (\Delta k \cdot z), \tag{9}$$

$$V_1(z) = V_{10}[\cos\ (\Delta k \cdot z) - j\zeta\ \sin\ (\Delta k \cdot z)], \tag{10}$$

where we have assumed $I_1(0) = 0$ and defined $\Delta k \equiv (k_s - k_f)/2 = \alpha_\mu \omega\delta/v_o$, $Z = (60\Omega)\ [\ell n(r_w/r_b)/\beta_o]/(-\zeta)$, $\zeta \equiv (1-\delta)/\alpha_\mu\delta$, $\delta \equiv \beta_o^2/(\beta_o^2-\alpha)$, and $\alpha_\mu \equiv (\alpha^2 + \alpha/\gamma_o^2)^{1/2}/\beta_o$. Note from Eqs. (9) and (10) that, unlike the interaction of a low density (classical) electron beam with a gap, I_1 and V_1 are partially in phase. This means that the balance of small signal energy involves not only the electromagnetic energy and the kinetic energy, but also the potential energy of the beam.

This simple analytic theory has been used to validate the initial results of our particle simulation studies. The code (CONDOR [36]) is two-dimensional, time-dependent and fully electromagnetic. Here, it was used first to interpret the experimental data which had been collected for the small diameter beam. It was then used to predict the performance of more recent experiments which used the large diameter beam.

To mimic the small diameter beam experiments as closely as possible, the simulation geometry [Fig. 5a] consisted of a 500 keV, annular IREB with beam radius $r_b = 1.9$ cm and beam current $I_o = 5$ kA propagating

along a metal cylinder of radius r_w = 2.4 cm. A static 10 kG axial magnetic field confines the IREB. A gap feeding a coaxial cavity 5.6 cm long is inserted into the drift tube. An infinite radial transmission line (not shown) is attached to the outer wall of this cavity and "pumps" rf energy into the cavity at a frequency f = 1.37 GHz, the resonance frequency of the cavity. The radial transmission line has an impedance of 15 ohms. At t = 0, the rf drive is turned on. At t = 6 ns, after the fundamental mode of the cavity has saturated, the beam current is ramped up, reaching its full value at t = 11 ns (5 ns rise). (Note that the cavity used in the simulation has an extremely low Q. This low value of Q has the advantage of reducing the time scales in the simulation.) The simulation continues until t = 20 ns.

For rf drives yielding gap voltage of amplitudes V_1 = 30 kV and V_1 = 6 kV, the axial distribution of the normalized rf current $I_1(z)/I_o$ in steady state was shown in Fig. 6. The temporal evolution of the beam current at a distance z = 28 cm from the gap center is shown in Fig. 7a for the V_1 = 30 kV case.

The agreement between the small signal [cf. Eq. (9)] and the simulation results as shown in Fig. 6 validates the applicability of the numerical code to the problem. The small signal theory has also been favorably compared with experiments [cf. Fig. 13 below].

B. Current Modulation in the Large Signal Regime

To confirm the experimental result that the current modulation may be substantially increased by inserting a second, undriven cavity downstream, we consider the geometry shown in Fig. 5b. The second cavity is tuned to the same frequency as the first cavity, and is placed at a

location where the current modulation (by the first cavity) reaches a maximum.

Using the same rf drive as that for Fig. 5a, we show in Fig. 7b the temporal evolution of the beam current a 6 cm downstream from the second gap, at which the gap voltage is 330 keV. The total current modulation there increases to 57%, including all harmonics. It continues to increase over the remaining 10 cm of propagation distance, reaching 85%. This is in excellent agreement with the experiments discussed in Section IV.

Phase space plots ($\beta\gamma c$ vs. z) of the electrons reveal important information. For example, we found that the bunching mechanism reached equilibrium very quickly. Figure 8 shows phase space pictures at different times but at a similar phase of three consecutive rf cycles. The three nearly identical plots show (i) that the mechanism is highly stable from cycle to cycle, (ii) that transients are unimportant, and (iii) no reflected electrons ($\beta\gamma < 0$) exist. The last point is significant because, unlike the earlier work [19], [20] on self oscillations, reflected electrons in our RKA are not required. Nor are they desired.

The phase locking between the external rf and the current modulation, implicit in the linear amplifier configuration, was tested for the fully modulated beam in this two-cavity geometry. We varied the phase of the input signal and observed a corresponding phase shift in the peaks of the current response [see Fig. 7b]. We found that as the input signal is shifted by π, the fully modulated beam is phase locked to within an error of $1.1 \pm 0.6\%$, in agreement with experimental observations [16], [17].

As in the conventional klystron, the harmonic content is considerable when the current modulation is on the order of the DC beam current. In the above simulation, as many as 11 harmonics were clearly observable in Fourier transforms of the current signal measured immediately downstream from the second gap. This high current modulation at the exit of the second gap is a manifestation of the "gate-effect" discussed in Section II.

The above simulations pertain to a small diameter beam. As was discussed in Section II, propagation of a high current beam demands the use of a large diameter annular beam. A question that was of considerable concern was whether enlarging the drift tube to accommodate the large diameter beam would diminish the bunching efficiency, as the cutoff frequency of the TM_{10} mode approaches the modulation frequency. While the rudimentary theory [35] has given some assurance, the simulation result given in Fig. 9 for a large diameter beam convincingly showed that the process of modulation is qualitatively similar to the small diameter beam. In Fig. 9, the first cavity was located at $z = 2.8$ cm and was driven by an external rf source (a radial transmission line of impedance 6.25 ohms), producing a gap voltage of 40 kV at 1.24 GHz. The second cavity was undriven and was located at $z = 36.8$ cm and tuned also at 1.24 GHz. The beam parameters were as follows: Current 16 kA, energy 600 keV (500 KeV after the first gap), diameter 12.6 cm, thickness 0.2 cm. The resulting rf current was $I_1 = 2.16$ kA at 30 cm from the first gap. This current modulation which was in good agreement with the linearized theory, excited the fundamental TEM mode of the second cavity to produce an oscillating voltage of 425 kV at the second gap. Note from Fig. 9 that there is also an instantaneous rise of the modulated current at the second gap

(indicative of the gate effect) and that the current modulation reaches 12.8 kA, 34 cm beyond the second gap. The phase stability, absence of reflected particles, etc., are also similar to the results with the small diameter beam.

There is one aspect in the particle simulation results which show that the modulation of a high current, large diameter beam might be different from the weaker, small diameter beam: A mechanism may exist which could limit the achievable current modulation. Specifically, we found that increasing the first gap voltage to 50 kV (from 40 kV) in Fig. 9 results only in a 3.1% increase in the peak modulation at z = 66.8 cm, from 12.8 kA to 13.2 kA, and further increase in the gap voltage does not significantly increase the current modulation. This feature was also revealed in the experiments of a high current beam. Several factors might contribute to the saturation in the current modulation. The presence of a biased voltage at the gap, for example, may reduce the critical current. This aspect will be examined in Subsection D below. Another possibility is that at high beam currents, the transit time effect, which reduces the effective gap voltage by the "gap transit time factor", can become very significant, as the potential due to the space charge of the beam would make the electrons to spend a longer time in the gap. [Recall that this space charge potential is significant--it provides the electrostatic insulation at the gap.] The modulating gap voltage, because of the gap factor, is then unable to produce as strong a current modulation as expected. Indeed, from phase space plots (not shown), we found that the beam energy was not modulated by the full 425 kV amplitude of the second gap voltage. We speculate, then, that it is these transit time effects, and the amount of current which can be transmitted across a gap with a

biased voltage, which place fundamental limits on the RKA efficiency. We shall return to these issues in Subsection D.

We have developed nonlinear theories which give the harmonic content of a highly modulated beam. We calculated the nonlinear propagation characteristics of the large amplitude space charge waves from a self-consistent formulation [17], [24]. We found that the slow space charge wave components strengthen the current bunching whereas the fast waves were relatively unaffected [Fig. 10]. We quantified the mechanism of increase in the bunching as illustrated in Fig. 3. We evaluated the gap transit time factor [25]. All of these analytic theories will not be repeated here.

C. Electrostatic Insulation and Magnetic Insulation Against Breakdown

The fact that gigawatt levels of rf power have been extracted without evidence of breakdown at the gaps can be attributed to the electrostatic insulation provided by the annular intense beam. The prevention of breakdown in the coaxial converter (or in the coaxial modulating cavity [Fig. 1]) is provided by the strong axial magnetic field [Fig. 4].

To probe further into these important areas, for electrostatic insulation, we perform simulations on the geometry shown in Fig. 9 in which the second gap is sealed. An annular intense beam is injected into a drift tube with E = 500 keV and I = 16 kA, with a current rise time of 5 ns, past the cavity. The gap voltage is controlled externally via a radial transmission line which has an impedance of 6.25 ohms. At t = 6 nsec, the externally applied voltage across the gap is increased linearly from zero to 400 kV over 4 nsec, and a second beam, I = 1 amp, E = 1 kV, is injected

continuously from the left-hand gap wall at $z = 2$ cm. The simulation continues until $t = 10$ nsec.

Voltage across the gap versus time is plotted in Fig. 11. Figure 11 also shows the leakage current crossing the gap as a function of time, measured at $z = 3.2$ cm. Initially, the rising DC current of the beam and the transmission line impedance cause a voltage drop which reaches 100 kV at $t = 5$ nsec. The effect of the externally applied voltage can be seen thereafter. The sudden increase in gap leakage current at $t = 8.6$ nsec indicates insulation for voltages less than 150 kV.

In this simple model, the 16 kA DC beam is shown to withhold a gap voltage of 150 kV beyond the breakdown voltage. As the limiting current is approached, the kinetic energy of the intense beam will be lowered near the gap, causing an increase in the net charge near the gap and a corresponding increase in the electrostatic insulation.

For magnetic insulation, we shall use analytic estimates to show that the axial magnetic field (~ 10 kG) used in the RKA experiment is sufficient to provide magnetic insulation against both electron and ion flows across the coaxial line of the rf converter.

Since the rf frequency, ω, is considerably less than the relativistic electron cyclotron frequency, we may treat the rf fields as essentially static as far as electron motions are concerned. Under this assumption, the relativistic Hull cut-off condition used in magnetron studies would give the magnetic field required for insulation. For a coaxial line of inner radius a and outer radius b the required magnetic field to provide magnetic insulation is given by [6], [7], [28]

$$B_c(\text{kG}) = \frac{1.07}{D(\text{cm})} \left\{ \left(\frac{Z_o}{10\Omega} \right) \left(\frac{I}{10\ \text{kA}} \right) + 0.098 \left[\left(\frac{Z_o}{10\Omega} \right) \left(\frac{I}{10\ \text{kA}} \right) \right]^2 \right\}, \quad (11)$$

where $Z_o = (60\Omega) \times \ell n(b/a)$ is the characteristic impedance of the coaxial line, I is the current flowing along it and $D \equiv (b^2 - a^2)/2a$ is the equivalent gap width. If a = 6.8 cm, b = 11.5 cm, then D = 6.3 cm and $Z_o = 31.53\ \Omega$. For a maximum current of $I_o + I_1 = 30$ kA, for instance, we obtain $B_c = 0.73$ kG. The imposed magnetic field is 10 kG, which is about 14 times higher than B_c, the value required for magnetic insulation. Thus, magnetic insulation against electron flow is virtually guaranteed.

For the ions, their cyclotron frequencies ω_{ci} are much smaller than the rf frequency, we may not use the static formula. Instead we solve the equation of motion and place an upper bound on their displacement (x) across the field line.

The ions satisfy the nonrelativistic force law, $m_i d\vec{v}/dt = e(\vec{E}_o + \vec{v} \times \vec{B}_o)$ where, for simplicity, we ignore the rf magnetic field in comparison with the external magnetic field, and $E_o = |\vec{E}|$ is the radial rf electric field. One can readily show that, if $\dot{x}(0) = 0$, and $x(0) = 0$,

$$|x(t)| < eE_o/m_i\omega_{ci}|\omega - \omega_{ci}|. \qquad (12)$$

For $m_i = 1840\ m_e$, $B_o = 10$ kG, $\omega_{ci} = 0.06$ GHz, and $\omega = 2\pi \times 1.3 \times 10^9 \text{sec}^{-1}$, Eq. (12) gives $|x| < 0.78$ mm if $E_o < 300$ kV/5 cm. Thus, magnetic insulation for the ions is also assured.

D. Limiting Current Across a Gap with a Biased Voltage and RKA Efficiency

The modulated beam yields its kinetic energy to rf when it is retarded by the decelerating voltage across the gap of the extraction section. One limit on the extraction efficiency is governed by the maximum current which can be transmitted through a gap without the formation of a virtual cathode. Naturally, the transmittable current is least when it is

subject to a retarding, biased gap voltage. This question is also of interest to diode (or inverse diode) physics, as it pertains to the maximum charges which can be held within the diode region.

For a one-dimensional, parallel plate gap and for a quasi-static gap voltage [i.e., transit time across the gap is much smaller than the period of the gap voltage], this limiting current can be calculated analytically. For a realistic gap with a more complicated geometry, such as the ones shown in Fig. 1 or Fig. 4, we know that no electron can be transmitted if the retarding (quasi-static) gap voltage exceeds the kinetic energy $(\gamma_e - 1)m_o c^2/e$ of the entering electrons. Inferring from the parallel plane gap model, we propose that, in general, the maximum current which can be transmitted across a retarding biased gap [held at voltage $(\gamma_e - 1)m_o c^2/e$] is [25]

$$I_c = 2I_s \cdot \left[f(\sqrt{\gamma_e \beta_e})\right]^2, \tag{13}$$

where the current scale

$$I_s \equiv C\,(m_o c^2/e)/T, \tag{14}$$

$\beta_e = (1 - \gamma_e^{-2})^{1/2}$ and $f(z) = \int_0^z dt\; t^2\,(1 + t^4)^{-1/2}$ whose properties are described in some detail in [37]. In Eq. (14), C is the capacitance (in vacuo) and T is the time required for light to traverse the gap. Equations (13) and (14) agree with the parallel plate gap of area A_o and separation D, in which case $C = A_o \varepsilon_o/D$ and $T = D/c$. Note that the current scale I_s introduced in (14) is also an adequate one to describe an entirely different system-- a thin annular beam of radius r_b drifting in a circular waveguide of radius r_w and length ℓ. In this geometry, $C = 2\pi\varepsilon_o \ell/\ell n(r_w/r_b)$ and $T = \ell/c$. Equation (14) then yields $I_s = 8.53\ \text{kA}/\ell n(r_w/r_b)$, the current

scale which enters repeatedly in our studies of this system and which appears as Eq. (2) above. Finally, for the present rf extraction experiment, C is the capacitance at the extraction gap and T = D/c where D is the gap length. For C = 6 picofarads and D = 2 cm, then I_s = 46 kA according to (14). If we take γ_e = 2, then Eq. (13) gives $I_c \simeq 25$ kA. We mention that this value of 25 kA is very close to the peak current observed in the experiment. The reduction in the limiting current by a biased gap voltage may be related to the saturation in current modulation that was observed in the particle simulations and in the experiments.

We shall now mention other factors which may affect the RKA efficiency, in addition the limiting current just explained. They include: the beam's energy modulation and its phase relation to the current modulation [38], the kinetic energy spread within the bunch, the partition between the kinetic and potential energy as the electrons enter the output gap, the substantial current modulation in higher harmonics and their (transient) interaction with the output gap voltage, geometrical effects, and the transit time factor which was mentioned above and its nonlinear modification due to the intense space charge of the beam. The interplay of all of these factors is, unfortunately, often nonlinear, local, and transient, so that a simple analytic scaling of the efficiency is unavailable at the moment.

Finally, we note that we have not found a method to tap the significant amount of the potential energy residing with the highly modulated beam. Such a procedure, if found, would be of considerable practical interest.

IV. Experiments

Two sets of experiments were conducted. The first one [16], [17] dealt with a small diameter beam ($r_b \simeq 2.35$ cm) which carried a current of 5 kA. In the second one [18], a large diameter ($r_b \simeq 6.6$ cm) beam carrying 16 kA current was used. In both experiments, the injection voltage was 500 kV, with a pulse length of 120 ns and the frequency of the external rf drive was 1.3 GHz.

The experiment with a small diameter beam was originally performed to demonstrate the efficient current modulation using an external rf source. It was this experiment which unearthed several interesting phenomena, such as great amplitude and phase stability, and the potential of electrostatic insulation. It led to the subsequent experiments of using a large diameter beam, and the extraction of a 3 GW of peak power rf radiation pulse from the fully modulated, large diameter beam.

We shall first describe the experiments with the small diameter beam, both at the small signal and nonlinear levels. We next report the more recent work on rf extraction using the larger diameter beam.

A. Modulation of a Small Diameter Beam

At the small signal level, only one single cavity was used. The experimental arrangement was shown in Fig. 12. It consisted of a foilless diode [39] emitting an annular IREB of radius $r_b = 1.9$ cm and thickness $= 0.3$ cm. A 10 kG quasi-DC magnetic field confined the IREB inside a metal tube of radius $r_w = 2.35$ cm. A gap feeding a coaxial cavity was inserted in the drift tube. The characteristic impedance of the cavity was 45Ω and its length was $L = 17$ cm corresponding to a resonance frequency of 410 MHz. Four thin Nichrome wires connected the inner wall of the coaxial cavity to its outer wall so as to reduce the Q of the cavity at 410 MHz. The wires

did not influence the Q of the cavity at the 1320-MHz resonance (Q > 1000). The presence of the wires shifted the first resonance from 410 to 610 MHz and reduced the Q to below 30. An external rf source (a magnetron) "pumped" microwave energy into the cavity for a duration of 3 μsec at a frequency f = 1328 MHz. Sometime during the 3 μsec period a Blumlein transmission line with an output of 500 kV energized the foilless diode for 120 nsec, and a ~ 5 kA electron beam was launched through the drift region. The base pressure in the drift region was $\leq 10^{-5}$ Torr.

For many applications the purity of the rf spectrum and phase locking are necessary requirements. The arrangement that was used to measure the degree of phase locking and the purity of the spectrum of the modulated IREB, is shown elsewhere [17]. We found in these experiments that the magnetron output and the modulated IREB were phase locked to better than 3° for 100 ns of the beam pulse, except perhaps during the rise time and fall time (~ 25 ns each) of the diode voltage. [See Fig. 6 of Ref. 17]. We also found that the frequency of the modulated IREB is the same as the frequency of the rf from the magnetron [16].

Four magnetic probes spaced 15 cm apart, the first of which was located 12 cm from the gap of the cavity, were used to analyze the electron beam that emerged from the cavity. (The magnetic probes and calibration arrangements were shown in Fig. 3 of Ref. [17].) Best fits to the results are in the form:

$$\text{for } V_o = 500 \text{ keV}, \quad 2I_1 = 450\left|\sin(0.0523z(\text{cm}))\right| \text{ Amps},$$

$$\text{for } V_o = 400 \text{ keV}, \quad 2I_1 = 425\left|\sin(0.0671z(\text{cm}))\right| \text{ Amps}.$$

The experimental result compared favorably with the theoretical prediction (Eq. (9)). Since the rf amplitude V_{10} was kept constant, the following

conclusions were drawn: (i) Z is insensitive to the IREB electron energy eV_o and (ii) Δk depends on the IREB electron energy eV_o.

Note that the amplitude I_1 depends linearly on V_{10}. We recorded I_1 as a function of the input rf power P. Since $P \propto V_{10}^2$ we get

$$I_1^2 = KP \text{ or } \log (I_1^2) = \log P + \log K \qquad (15)$$

where K is a constant that does not depend on V_{10} and I_1. Figure 13 displays experimental results as log (I_1^2) vs log (P). The slope of the best fit straight line is unity in accordance with Eq. (15). From Fig. 13 and Fig. 6, we see that there is excellent agreement between experiment, theory, and simulation.

To modulate the beam much beyond the small signal level, one would require a gap voltage of the order of hundreds of keV, if the small signal theory is used as a guide. This level of gap voltage corresponds to an input rf power greater than 20 MW if only a single cavity was used [Fig. 12]. Since an rf source with this kind of power was not available, we used, instead, the partially modulated IREB to energize a second coaxial cavity [Fig. 14] and to generate a high oscillating voltage (~ 150 kV) on its gap. The gap of the second cavity was inserted in the drift tube at an axial position for which I_1 was maximum (29 cm). The second cavity with a $Q > 2000$ was tuned to the frequency $f = 1.328$ GHz $\pm$ 1 MHz. The IREB that emerged from the second cavity was highly modulated. The peak current in the bunches was
~ 80% of the DC current [Fig. 15]. This level of current modulation is consistent with the numerical simulation reported in Section II.

In a different experiment the second cavity was replaced by a variable length cavity. With this cavity, the resonance frequency could be

varied between 800 MHz and 2.9 GHz. The cavity Q was $\lesssim 400$ (at a frequency of 1.3 GHz). Because of the low Q, the input impedance of the gap was complex, i.e., $Z_s = R_s + jX$, even at frequencies close to the resonance frequency. It was found that by raising the magnetron rf power, no disruption of the IREB current was observed. Moreover, the rf current amplitude of the IREB increased by a factor of ~ 1.6 to $2I_1 = 7$ kA. Figure 16 shows the experimental setup. It also shows the variation of $2I_1$ as a function of the resonance frequency of the second cavity and of the position where the measurements were taken.

Previous experimental investigations of the generation of modulated IREBs showed that when I_1 is of the order of I_o, harmonics of the main frequency appeared. Here, harmonics are not shown in the spectrum of the current. The reason is the high attenuation of the signal cables and oscilloscopes at frequencies above 1.3 GHz.

The presence of the second and third harmonics in the current modulation was detected by mixing the signals from magnetic probes with local oscillators working at frequencies ~ 2.5 and ~ 3.8 GHz. The rf current at the second harmonic was measured relative to the rf current at the fundamental. When the configuration with high Q cavities was used, the rf current ratio of the second harmonic to the fundamental was 0.3. This was found to be in qualitative agreement with the analytic estimate for the nth harmonic current modulation [17]

$$|I_n(z)| \simeq 2\, I_o |J_n((n\, V_{10}/Z\, I_o)\sin(\Delta k \cdot z))| \qquad (16)$$

where the symbols were defined in Eq. (9).

As was found in an earlier work by the authors, the spectrum of modulation can be modified by propagating the modulated IREB through

additional cavities. A similar approach was used here to change the level of the current of the second harmonic. For example, when a third cavity tuned to a 2.6 GHz was placed downstream of the second cavity, the ratio of the second harmonic current to the fundamental was increased to 0.8. When the third cavity was tuned to ~ 2 GHz this ratio was ~ 0.1.

B. Modulation of Large Diameter Beam

The modulation of a large diameter, high current beam was not as straightforward as a small diameter beam. There are several reasons, some of them were anticipated, while others were discovered only after considerable experimentation and numerical simulation [see Section IIID above]. An obvious problem is that as the diameter of the drift tube is increased to accommodate a large diameter beam, the cutoff frequency of the drift tube may approach the modulating frequency. The electric field would no longer be confined only at the gap region, and the modulating cavities are not isolated electromagnetically. This would be detrimental to beam modulation and is one of the reasons why the present modulation experiments (at 1.3 GHz) are limited to a tube diameter not more than 14 cm when we used a hollow drift tube configuration. Once the gap provides a strong, localized, velocity modulation of the beam, the current modulation then evolves in much the same way as the small diameter beam.

A second problem is that when the drift tube radius becomes large, the mode in the coaxial cavity may not be a pure TEM mode and care is to be exercised to ensure that the gap field corresponds to the desirable mode. This was also indicated from results of the SUPERFISH numerical code [40]. Lastly, as explained in Section IIID, the high current which accompanies the large diameter beam tends to retard the electrons, and could reduce the gap transit time factor to a value significantly less than unity. This may

limit the maximum current modulation, and hence the efficiency, when a large diameter, high current beam is used.

We summarize below our experimental studies on the modulation of a large diameter beam, first in the small signal regime using a single cavity and later in the nonlinear regime, where a highly modulated beam is obtained with the addition of a second, undriven cavity downstream.

The parameters of the large diameter annular beam are: I_o = 16 kA, r_w = 7 cm, r_b = 6.6 cm, beam thickness = 0.3 cm. It is generated from the same foilless diode arrangement as with the smaller beam reported in the preceding subsection: A voltage pulse of 500 kV, pulse length 120 nsec is injected into a drift tube, which is immersed in a 10 kG solenoidal magnetic field and evacuated to a base pressure less than 10^{-5} torr. Again, a gap feeding a cavity was inserted in the drift tube. This cavity supported many resonance modes, one of which was a hybrid of a coaxial TEM and TM modes with a frequency of 1.328 GHz. The "Q" factor of the cavity was 1100. An external RF source pumped power into the cavity for a duration of 1 μsec. The electrical parameters of the cavity were calculated using the SUPERFISH computer code. We found: (1) that the gap voltage, V_g was half as high as the largest voltage in the cavity, and (2) the electrical parameters of such a cavity constructed of copper (power dissipation P, energy stored W, quality factor Q and gap voltage V_g).

Using these parameters one can calculate the relationship between input power and V_g for any real cavity of the same geometry. It is easy to show that for two cavities (subscript 0 and 1) of the same geometry but with different Qs the following relationship exists:

$$V_{g1} = V_{go} \left(\frac{P_1 Q_1}{P_o Q_o} \right)^{1/2} .$$

From the SUPERFISH code one calculates that for a cavity made of copper, $Q = 39700$ and for $P_o = 5.25 \times 10^4$ W one gets $V_{go} = 87$ kV, and $V_{g1} = 63.2\ P_1^{1/2}$. The power injected into the cavity in the experiment was typically 0.5 megawatt, giving $V_{g1} = 45$ kV.

Sometime after the voltage at the gap reached its maximum value a Blumlein transmission line energized the diode, resulting in IREB propagation across the gap of the cavity.

The oscillatory voltage V_{g1}, imposed on the gap partially modulated the IREB generating at point z an RF current $I_1(z)$ and RF voltage $V_1(z)$. The latter quantities are given by Eqs. (9) and (10), respectively, in which V_{10} is replaced by MV_{g1}. Here, $M < 1$ is the gap factor due to the finite transit time effect. From the particle simulation code, CONDOR, we found $M = 0.6$. Together with the experimental parameters, we found $Z = 16\Omega$, $\Delta k = 0.039\ cm^{-1}$, $\zeta = -0.35$. Using these parameters for $V_1(z)$ and $I_1(z)$, as given in Eqs. (9) and (10), we obtain a theoretical maximum value of $I_1 = 1800$ Amps at a distance 40 cm downstream. Experimentally, we found that the IREB RF current reached the maximum at a point $z = 35$ cm. At this point $I_1 = 1750$ Amps, in excellent agreement with the above estimates. On the other hand, CONDOR gave $I_1 = 3200$ Amps at a distance of 44 cm from the gap, using an oscillating voltage of 50 kV amplitude. We believe that the discrepancies came from assumptions made on the values of the experimental parameters, e.g., the geometry of the cavities in the simulation differ from those used in the experiment.

To increase the current modulation using the same rf drive, we insert a second gap, (which is undriven) at 35 cm downstream of the first gap. This gap was feeding a coaxial cavity of low impedance, Z_c = 10 ohms. The length of the cavity was 3/4 λ ($f = (c/\lambda) = 1.328$ GHz). In this cavity, 4 resistive wires were placed radially, connecting the inner and outer conductors. The purpose of the wires was to reduce the "Q" of the cavity at resonance frequencies lower than 1.328 GHz.

The geometry of the second cavity was chosen such that:

(a) The ratio of gap voltage to peak voltage was maximized.

(b) The shunt impedance of the cavity, R_s, was maximized. Using the SUPERFISH computer code and experimenting with various cavities we found the best cavity geometry that fulfilled the above conditions. For this cavity the ratio of the gap voltage to the peak voltage was 0.8. The shunt impedance of this 3/4 λ cavity was $R_s = 0.8(3\pi/4)Q(Z_c)$.

When a modulated IREB traversed such a cavity, an induced RF voltage appeared on the gap, increasing the depth of the current modulation by a gain factor GA which reached maximum at an axial position $L = 1/\Delta k$ cm [17]:

$$GA = M^2(R_s/Z + \zeta). \tag{17}$$

GA was evaluated and found to be GA = 30.

Using this gain an RF current exceeding the DC current was obtained. The result indicates that a nonlinear treatment is needed to explain experimental observations.

The IREB current downstream from the second gap was found [Fig. 17] to have the following time dependence

$$I = I_o + I_1 \cos(\omega t) + \ldots\ldots, \tag{18}$$

with I_1 reaching a maximum value of 8.5 kA at a distance 39 cm from the second gap.

Large changes in the RF power input into the first cavity affected I_1 only marginally. Hence, we conjectured that saturation had been achieved. But unlike our small diameter beam experiment in which we found $I_1/I_o = 0.8$, here $I_1/I_o = 0.5$ was obtained and could not be further increased. Although saturation may be a distinct possibility [see Section IIIB,D], it is also possible that the current measurements (which were inferred from magnetic field measurements via a DC approximation) may not actually represent the true rf current on a bunched beam IREB current. Using Linear theory we estimated that, as $I \approx I_c$ [18, 25],

$$I_1 \text{ (REAL)} \approx I_1 \text{ (MEASURED)} \times \frac{2}{1 + \varepsilon}, \tag{19}$$

where

$$\varepsilon \approx \exp \left\{ \frac{- 4\pi \left(\frac{r_w - r_b}{\lambda} \right)}{\beta_o (1 - I/I_c)} \right\} . \tag{20}$$

I_1 (real) is the real RF current, I_1 (measured) is the measured RF current, and I_c is the critical current in the drift tube. Substituting the experimental results, one gets

$$I_1 \text{ (real)} = 1.4 \times I_1 \text{ (measured)} = 12 \text{ kA}$$

Note that Eq. (19) was not solved self-consistently since we substitute $I = I_o + I_1$ (real) and that only linear theory was used to derive Eq. (20). We can conclude that the measured RF current is probably lower than the value of the true RF current.

C. RF Extraction from the Modulated Large Diameter Beam

It is well known that RF power can be extracted from a modulated electron beam. Since the electrons in an IREB are relativistic there will be less reduction in particle velocity (or IREB current) while electrons are losing energy. Hence, we can model the modulated IREB as a constant current source I [cf. Eq. (18)].

The interaction of this current source with an RF structure can lead to transfer of power from the electrons to a load. The structure can be described as an electrical element with an input impedance of Z_{in}. A voltage V_{in} will develop across the electrical element

$$V_{in} = Z_{in} \times I \tag{21}$$

To extract maximum RF power from the IREB, with a frequency $\omega/2\pi$, the following requirements must be fulfilled:

(a) $V_{in} < V_o$, otherwise the constant current source model for the IREB will not be correct and the flow of IREB will be disrupted.

(b) Z_{in} has to be real at the frequency of the extracted RF. At this frequency, Z_{in} is denoted as $Z(\omega)$.

(c) The absolute value of Z_{in} at other frequencies has to be smaller than $Z(\omega)$.

(d) $Z_{in} = 0$ at low frequencies of the order of $1/T$ where T is the beam duration (in the experiment T = 120 nsec).

In order to transport this power into a load an additional requirement has to be fulfilled:

(e) Elimination of RF breakdown.

The device shown in Fig. 1 addresses all of the above requirements. The RF extraction section of the device consists of the following parts:

(1) A high voltage gap across which the electron bunches are moving and losing energy. Electrostatic insulation is of importance here since voltages of the order of 0.5 MV will appear across the gap when efficient extraction of RF power is taking place. The maximum current that can propagate across the gap is estimated from Eq. (13), and found to be of order 25 kA.

(2) The gap which is connected to an antenna via a coaxial transmission line. The center conductor is supported by thin metallic rods which are terminated in $1/4\lambda$ cavities [Fig. 1]. The axial positions of these rods are the locations of zero-amplitude node points of standing waves. The total impedance of the parallel circuits formed by the rods is large and can be considered infinite for the 1.328 GHz component of the RF current. This impedance is lower for higher frequencies and zero for the low frequency and the DC components of the current.

(3) The last part of the converter was the antenna which has a conical shape for both the inner and outer parts. The length of the antenna was a few wavelengths. A lucite plate 5 cm thick acted as a window. It has a diameter of one meter and attenuates ten per cent of the rf power. At the window, the rf is in the TM_{01} cylindrical mode.

At the far end of the inner conductor in the RF converter, an RF "obstacle" in a shape of a disc was placed. The axial position and diameter of the disc could be varied. This part of the converter was modeled using transmission line calculations. Figure 18 shows the model.

The gap is represented by a capacitor of value C_o, the obstacle is represented by a capacitor C, the load is R_1 and the transmission line is of length ℓ and impedance Z_o. Realistic values for the parameters in the model were found in the following way: C_o was calculated from the shift of the resonance frequency of an ideal 1/4λ cavity with a similar gap geometry

$$\frac{1}{j\, Z_o\, tg\left(\frac{\pi}{2}\,\frac{f}{f_o}\right)} + j2\pi f C_o = 0, \qquad (22)$$

where f_o is the resonance frequency of the ideal 1/4λ cavity and f is the resonance frequency of a cavity with a gap of capacitance C_o. We found that C_o = 6pF.

The value for R_1 was assumed to be equal to Z. The reason for this was that when the obstacle was removed the VSWR was close to 1 over a wide range of frequency. C and ℓ were left as free parameters that we tried to optimize so that the input impedance Z_{in} = R + jX would be real at 1.328 GHz and of a value between 50 to 100 ohms. Note that we can have a series of solutions for ℓ separated by 1/2 wavelength. Figure 19 displays one solution for R and X. We found that ℓ had to be chosen with great accuracy and that the value of R increased when C was increased.

The model is only qualitative in nature since it does not take into account the existence of non-TEM modes at various places inside the converter.

A set of experiments was performed in which ℓ and C were adjusted so as to get maximum radiated power. With optimum conditions we observed radiated power (outside the horn) of 2.7 gigawatts [Fig. 20]. The IREB parameters were: 16 kA current and 500 kV voltage. The separation between

the first gap and second gap of the modulating cavities was 34 cm, and that between the second gap and the gap of the rf convertor [Fig. 1] was 31 cm.

The total radiated power was derived in two ways:

(1) The radiation pattern was measured and the power/cm^2 was obtained. The total radiated power was then obtained by integration.

(2) An external RF source of 50 ohms impedance was connected at the gap via a slotted transmission line. The electrical parameters of the converter were adjusted to achieve a VSWR of 1 measured by the slotted line. This implied that the converter acted as a matched load to the external source. Measuring the input power and the response of a receiving horn yield the calibration factor. Excellent agreement (to within 10%) between the two power measurements was achieved.

In the power measurements the receiving horn was connected to a 7103 Tektronix 1 GHz oscilloscope. All of the electrical components that were used in measuring the power were calibrated whenever a series of experiments was performed.

From Fig. 20 one can see that the radiated RF power had a slow rise time, about 60 nsec. It takes a time τ to fill a cavity with RF

$$\tau \simeq \frac{2}{M} \tau_{1/e}; \quad \tau_{1/e} = 2Q/\omega,$$

where M is the gap factor due to finite transit time of the electrons across the gap [18, 25].

Experimentally, we found $Q \simeq 80$; hence, $\tau \simeq 60$ nsec. At low Rf output power the decay time of the power also lasted 60 nsec. At high power the decay time was shorter and a power of 2.7 gigawatts was maintained for approximately 30 nsec. We speculate that the gap lost its

electrostatic insulation due to the drop of the current at the end of the IREB pulse [Fig. 17].

On occasions when the current was terminated earlier, due to flash-over in the diode, the fall time of the current and the duration of the RF power was even shorter.

V. Discussions

In spite of the progress made toward understanding these devices, many issues remain unanswered on this relatively new subject of an RKA driven by a modulated intense relativistic electron beam. They range from the basic physics of beam modulation to the technological developments which are required to make this device useful for practical applications. Here, we shall examine some of these issues.

The experiences we have accumulated thus far leave little doubt that the space charge effects of the IREB are responsible for at least two distinctive advantages of this RKA configuration: electrostatic insulation and efficient current bunching. There are, however, also indications that further increasing these effects (i.e., higher current) will set limits on the achievable current modulation. First, the gap transit time factor reduces the beam-gap interaction significantly when the beam current becomes very high. Second, when the gap is biased to retard the beam, the limiting current is significantly reduced. For a high DC current, this implies a low current modulation to avoid the formation of the virtual cathode during the retarding phase of the gap voltage. The dual role of the DC space charge - on the one hand enhancing the bunching efficiency and on the other hand limiting the beam gap interaction when the beam current becomes too high - is clearly one of the key factors in the determination

of the RKA efficiency. At the moment, reliable scalings for RKA efficiencies are unavailable. In addition, the potential energy of the IREB, while performing the wonderful role in the electrostatic insulation, is wasted as far as energy extraction is concerned (unless it can somehow be tapped). These key physics issues need to be examined if rf output much beyond the 3 GW level already achieved (at 1.3 GHz) is desired.

The next question is the scalability to frequencies beyond 10 GHz. The hollow drift tube configuration studied in this paper is unlikely to achieve power level in the GW range at such high frequencies, as the drift tube radius is always constrained to be less than 1 cm, so that the modulation frequency is below cutoff. One possible solution, which we have studied, is to propagate the large diameter beam inside a coaxial drift tube, whose inner wall and outer wall are sufficiently close to each other. Such a configuration may be highly overmoded, however. For example, it is well known that TEM modes exist in a coaxial geometry. It appears then that mode control and structure tolerance are perhaps the most important issues in using a large diameter annular beam to generate rf beyond the 10 GHz range. We are currently planning an experiment working at the intermediate frequency of 3.6 GHz.

In the RKA experiments which we have conducted thus far, the rf is radiated into the atmosphere. In many applications (e.g., rf accelerators), radiation in the rectangular TE_{01} mode would be required. Mode conversion from the TEM coaxial to TE_{01} rectangular mode necessarily takes place in a strong applied magnetic field in such a way that this magnetic field is perpendicular to the rf electric field to ensure magnetic insulation. One such mode converter is proposed in Ref. [18], where radial

fins are introduced from the center conductor of the coaxial line [Fig. 21]. The radial dimensions of the fins increase axially, and, upon reaching the outer conductor of the coaxial line, the cross sectional areas which the fins divide are adiabatically transformed into cross-sections of rectangular waveguides. The number of rectangular waveguides could be made large for a large diameter coaxial line so that the rf power per waveguide is below the breakdown level.

Perhaps the most important issue which requires attention before the device could enjoy a wide range of applications is with repetition rate capability. While the branched magnetic switching, invented by Birx et al. [22], has the potential of solving the single pulse problem, rep-rating a pulsed power system (and solving the associated problem of electron emission), by itself, is an outstanding problem in its own right. Research and development on this problem may require an even greater effort than that of actually building the RKA once such a source becomes available. For it remains a fact that a modulated intense beam can be converted to rf with good efficiency.

We shall not discuss here the applications once the aforementioned problems are solved. We only mention a few: compact rf electron accelerators [41]-[44], and ion accelerators with their uses in driving free electron lasers and in breeding fissionable material, plasma heating, nuclear radiography, medical applications and other applications [45].

Acknowledgment

This work was supported by the Strategic Defense Initiative Organization, Office of Innovative Science and Technology, and managed by the Harry Diamond Laboratory. The early phase of this work was supported by the Department of Energy under Contract No. DE-AI05-86-ER13585.

References

1. P. B. Wilson, in Physics of High Energy Accelerators, edited by R. A. Carrigan, F. R. Huson, and M. Month, AIP Conference Proceedings No. 87 (American Institute of Physics, New York, 1982), pp. 450-563.

2. See, e.g., Proceedings of the 1989 IEEE Particle Accelerator Conference, ed. F. Bennett and L. Taylor, IEEE Cat. No. 89 CH2669-0.

3. Proceedings of International Workshop on the Next Generation Collider, Standford Linear Accelerator Center (Nov 29 - Dec 3, 1988); Also, in Advanced Accerator Concepts, AIP Conference Proceedings No. 193 ed. Chan Joshi, (American Institute of Physics, New York, 1989).

4. See, e.g., Proc. Society Photo-Optical Instrum. Engineers, Vol. SPIE-1061, "Microwave and Particle Beam Sources and Directed Energy Concepts", Ed. Howard E. Brandt, 1989.

5. A. Staprans, E. W. McCume, and J. A. Puetz, "High Power Linear Beam Tubes", Proc. IEEE 61, pp. 299-330. (1973), and references therein.

6. G. Bekefi and T. J. Orzechowski, "Giant microwave bursts emitted from a field-emission, relativistic electron beam magnetron", Phys. Rev. Lett. 37, pp. 379-382 (1976); A. Palevsky and G. Bekefi, "Microwave emission from pulsed relativistic e-beam diodes II. The multiresonator magnetron", Phys. Fluids 22, 986 (1979) S. C. Chen, G. Bekefi, R. J. Temkin, and C. deGraff, p. 157, Ref. [4].

7. G. Benford, in "High Power Microwave Sources", Chapter 8, Eds. V. L. Granatstein and I. Alexeff, Artech House, Inc., Norwood, MA (1987); also in Ref. [4].

8. S. Burkhardt, R. Scarpetti, and R. L. Lundberg, "A Virtual-Cathode Reflex Triode for High-Power Microwave Generation", J. Appl. Phys., Vol. 59, p. 28, 1985; H. A. Davis, R. R. Bartsch, L. E. Thode, E. G. Sherwood, and R. M. Stringfield, "High-Power Microwave Generation from a Virtual Cathode Device", Phys. Rev. Lett., Vol. 55, p. 2293, 1985; J. Benford, H. Sze, W. Woo, and B. Harteneck, "Virtual-Cathode Oscillator Emission by a Pinched Diode", Phys. Rev. Lett., Vol. 56, p. 27, 1986.

9. See, e.g., V. L. Granatstein and A. Mondelli, in Physics of High Energy Accelerators, AIP Conference Proceedings No. 153, Eds. M. Month and M. Dienes, p. 1501 (AIP, New York); also, S. H. Gold, W. M. Manheimer, W. M. Black and A. W. Fliflet, p. 201 of Ref. [4].

10. Y. Carmel, K. Minami, R. A. Kehs, W. W. Destler, V. L. Granatstein, D. Abe, and W. L. Loui, "Demonstration of efficiency enhancement in a high-power backward wave oscillator by plasma injection", Phys. Rev. Lett. 62, pp. 2389-2392 (1989).

11. P. B. Wilson, private communication.

12. M. A. Allen, O. Azuma, R. S. Callin, H. Deruyter, K. R. Eppley, K. S. Fant, W. R. Fowkes, W. B. Herrmannsfeldt, H. A. Hoag, R. F. Koontz, T. L. Lavine, T. G. Lee, G. A. Loew, R. H. Miller, R. B. Palmer, J. M. Paterson, R. D. Ruth, H. D. Schwarz, A. E. Vlieks, J. W. Wang, P. B. Wilson, W. A. Barletta, J. K. Boyd, T. Houck, T. J. Orzechowski, D. S. Prono, R. D. Ryne, G. A. Westenskow, S. S. Yu, D. B. Hopkins, A. M. Sessler, J. Haimson and B. Mecklenburg, "Relativistic Klystrons", in Ref. [2]; also in Lawrence Livermore National Laboratory, UCRL 98843 (June 1, 1988); Stanford Linear Accelerator Center publication 4801 (March, 1989).

13. J. LeDuff, in Ref. [3].

14. D. Birx, D. Goodman, R. Klinkowstein, and J. Mangano, private communication.

15. M. A. Allen et al., "Recent Progress in Relativistic Klystron Amplifiers", Stanford Linear Accelerator Center Publication No. 5070 (August, 1989); also Lawrence Livermore National Laboratory, UCRL 101688 (August, 1989).

16. M. Friedman and V. Serlin, "Modulation of Intense Relativistic Electron Beams by an External Microwave Source", Phys. Rev. Lett., Vol. 55, pp. 2860-2863, 1985.

17. M. Friedman, J. Krall, Y. Y. Lau, and V. Serlin, "Externally Modulated Intense Relativistic Electron Beams", J. Appl. Phys., Vol. 64, pp. 3353-3379, 1988.

18. M. Friedman, J. Krall, Y. Y. Lau, and V. Serlin, "Efficient Generation of Multi-Gigawatt RF Power by a Klystron-Like Amplifier", Rev. Sci. Instrum. Vol. 61, pp. 171 - 181 (1990).

19. M. Friedman, V. Serlin, A. Drobot, and L. Seftor, "Propagation of Intense Relativistic Electron Beams Through Drift Tubes with Perturbed Walls", Phys. Rev. Lett., Vol. 50, pp. 1922-1925, 1983.

20. M. Friedman, V. Serlin, A. Drobot, and L. Seftor, "Self Modulation of Intense Relativistic Electron Beams", J. Appl. Phys., Vol. 56, pp. 2459-2475, 1984.

21. M. Friedman, V. Serlin, A. Drobot, and A. Mondelli, "High-Power Modulated Intense Relativistic Electron Sources with Applications to RF Generation and Controlled Thermonuclear Fusion", IEEE Trans. Plasma Sci., Vol. PS-14, pp. 201-214, 1986.

22. D. L. Birx, E. J. Lauer, L. L. Reginato, D. Rogers, Jr., M. W. Smith, and T. Zimmerman, Proceedings of the 3rd IEEE International Pulsed Power Conference, Albuquerque, NM, June 1981, edited by T. H. Martin and A. H. Gunter (IEEE, New York, 1981), pp. 262-268, IEEE Cat. No. 81CH1662-6.

23. J. Krall and Y. Y. Lau, "Modulation of an Intense Beam by an External Microwave Source: Theory and Simulation", Appl. Phys. Lett., Vol. 52, pp. 431-433, 1988.

24. Y. Y. Lau, J. Krall, M. Friedman and V. Serlin, "Nonlinear Space Charge Waves on an Intense Relativistic Electron Beam", IEEE Trans. Plasma Sci., Vol. PS-16, pp. 249-257 (1988).

25. Y. Y. Lau, J. Krall, M. Friedman and V. Serlin, "On Certain Theoretical Aspects of Relativistic Klystron Amplifiers", pp. 48-59, of Ref. [4].

26. M. Friedman and V. Serlin, "Electrostatic Insulation of a High Voltage Gap", IEEE Trans. Electr. Insul. Vol. EI-23, pp. 51-54 (1988).

27. M. Friedman and V. Serlin, "Behavior of High Voltage Gaps in the Presence of Large Space Charge Fields", J. Appl. Phys. 58, pp. 1460-1465 (1985).

28. See, e.g., R. B. Miller, An Introduction to the Physics of Intense Charged Particle Beams, New York: Plenum, 1982, ch. 3.

29. J. D. Lawson, The Physics of Charged Particle Beams, Second Edition, Oxford University Press, p. 108 (1988); R. C. Davidson, Theory of Non-Neutral Plasmas, (Benjamin, New York, 1974).

30. V. S. Voronin, Yu. T. Zozulya, and A. N. Lebedev, "Self-consistent steady states of the flow of relativistic electrons in a drift space", Sov. Phys. Tech. Phys., Vol. 17, pp. 432-436 (1972).

31. If one instead uses a high energy beam, its "stiffness" would make it difficult to bunch longitudinally. It was suggested (by W. K. H. Panofsky) that by modulating the beam in the transverse direction and by bending the beam path with an external magnetic field, ballistic bunching may occur for a high energy beam after the modulated electrons traverse different circular paths. Experiments along this line are being planned (T. Godlove and F. Mako, private communciation). A somewhat different concept which also utilized the circular paths of electrons was proposed by Y. Y. Lau, "Collective Interaction Klystron", Phys. Rev. Lett., Vol. 53, pp. 395-398, 1984. The latter concept was currently under experimentation by John Pasour and Tom Hughes, as reported in Ref. [2] above.

32. R. J. Briggs, "Space-Charge Waves on a Relativistic Unneutralized Electron Beam and Collective Ion Acceleration", Phys. Fluids, Vol. 19, pp. 1257-1258, 1976.

33. M. V. Chodorow (private communication) suggested that the lack of dispersion in the space charge waves may be a result of the proximity of the annular beam to the wall. Whatever electromagnetic field that is set up at a particular location by the image charges on the wall depends only on the instantaneous distribution of the space charges on the beam at that location.

34. See eg., M. V. Chodorow and C. Susskind, Fundamentals of Microwave Electronics (McGraw-Hill, New York, 1964); J. W. Gewartowski and H. A. Watson, Principles of Electron Tubes (Van Nostrand, New York, 1965).

35. Y. Y. Lau, "Some Design Considerations on Using Modulated Intense Annular Electron Beams for Particle Acceleration", J. Appl. Phys., Vol. 62, pp. 351-356, 1987.

36. CONDOR is an extension of the MASK code developed by A. Palevsky and A. Drobot, Proc. 9th Conference on Numerical Simulation of Plasmas, Northwestern University, Evanston, IL, 1980 (unpublished).

37. Y. Y. Lau, "Effects of Cathode Surface Roughness on the Quality of Electron Beams", J. Appl. Phys., Vol. 61, pp. 36-44, 1987.

38. The complexity in beam-gap interactions, even for a low current beam where space charges are neglected, is evident in a recent paper by Z. D. Parkas and P. B. Wilson, "Dynamics of an Electron in an RF Gap". SLAC Publication No. 4898 Rev. (June, 1989, to be published.)

39. M. Friedman and M. Ury, "Production and Focusing of a High Power Relativistic Annular Electron Beam", Rev. Sci. Instrum., Vol. 41, pp. 1334-1335, 1970.

40. K. H. Halbach and R. F. Holsinger, Lawrence Berkeley Laboratory Report No. LBL-5040, 1976.

41. M. Friedman and V. Serlin, "Particle Accelerators Powered by Modulated Intense Relativistic Electron Beams", Appl. Phys. Lett. 49, pp. 596-598, (1986).

42. M. Friedman, J. Krall, Y. Y. Lau, and V. Serlin, "Electron accelerators driven by modulated intense relativistic electron beams", Phys. Rev. Lett. 63, pp. 2468-2471, (1989).

43. J. Krall, V. Serlin, M. Friedman, and Y. Y. Lau, "Simulation Studies of Particle Acceleration Powered by Modulated Intense Relativistic Electron Beams", Part. Accel. vol. 25, pp. 43-56 (1989); V. Serlin, M. Friedman, Y. Y. Lau and J. Krall, in p. 473 of Ref. [4].

44. M. A. Allen et. al., "High-Gradient Electron Accelerator Powered by a Relativistic Klystron", Phys. Rev. Lett. 63, pp. 2472-2475 (1989).

45. "High Power Microwave", "Pulsed Power", and "Phase Array" are recently listed as three of the twenty-two critical technologies by the U. S. Departments of Energy and Defense. See Physics Today, Vol. 42, No. 9, p. 68 (September, 1989).

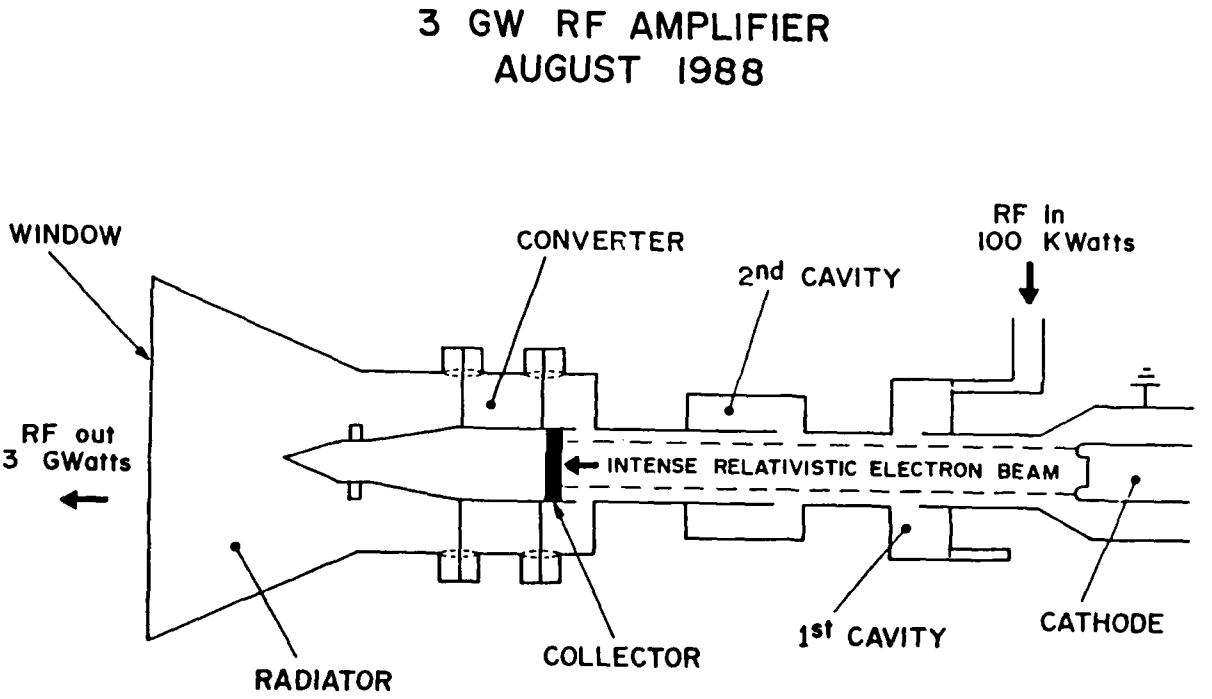

Fig. 1 The experimental arrangement of the gigawatt relativistic klystron amplifier.

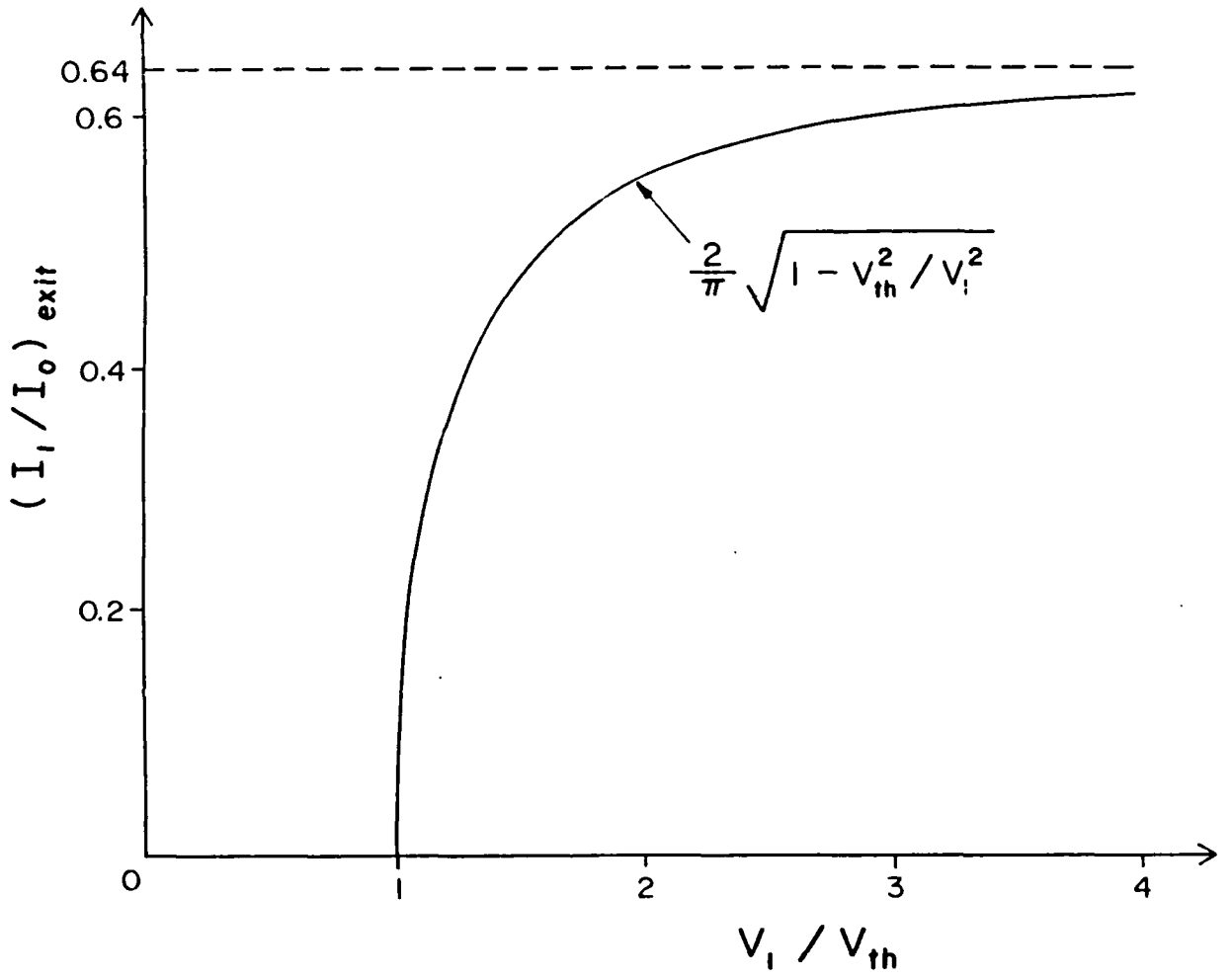

Fig. 2 Current modulation at the gap exit as a function of modulating gap voltage.

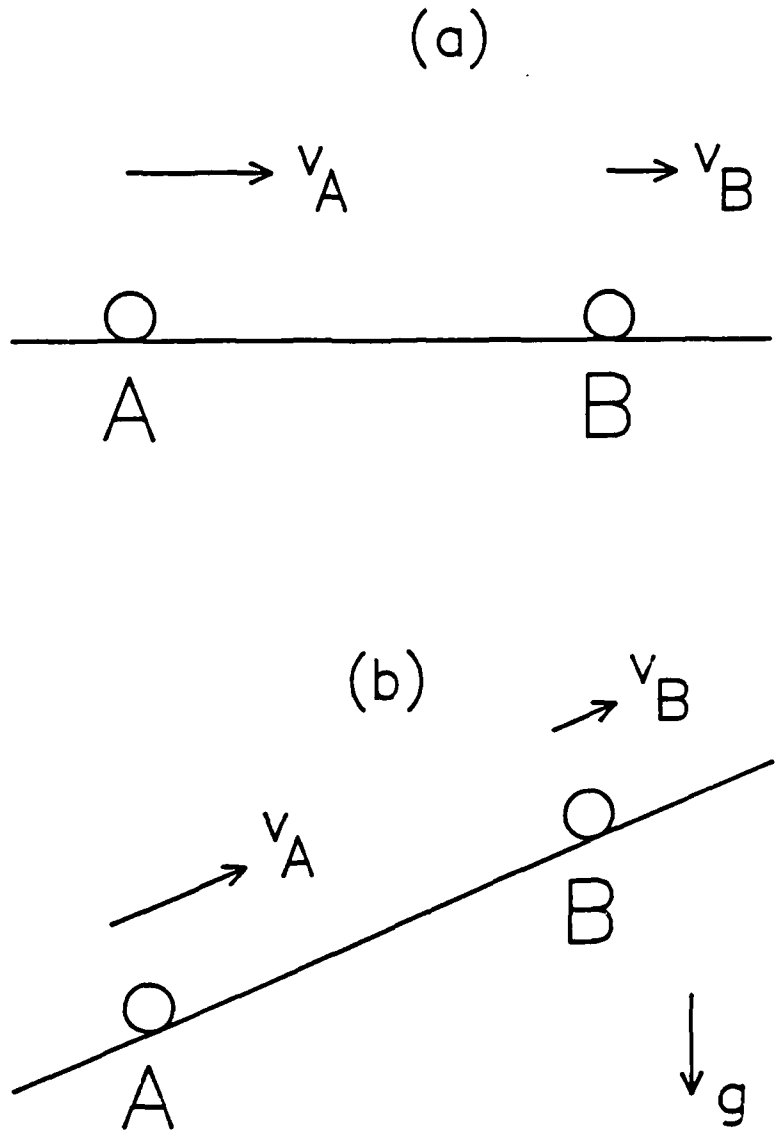

Fig. 3 Comparison of ballistic bunching in (a) the classical klystron model and in (b) a simple RKA model where a retarding potential is present.

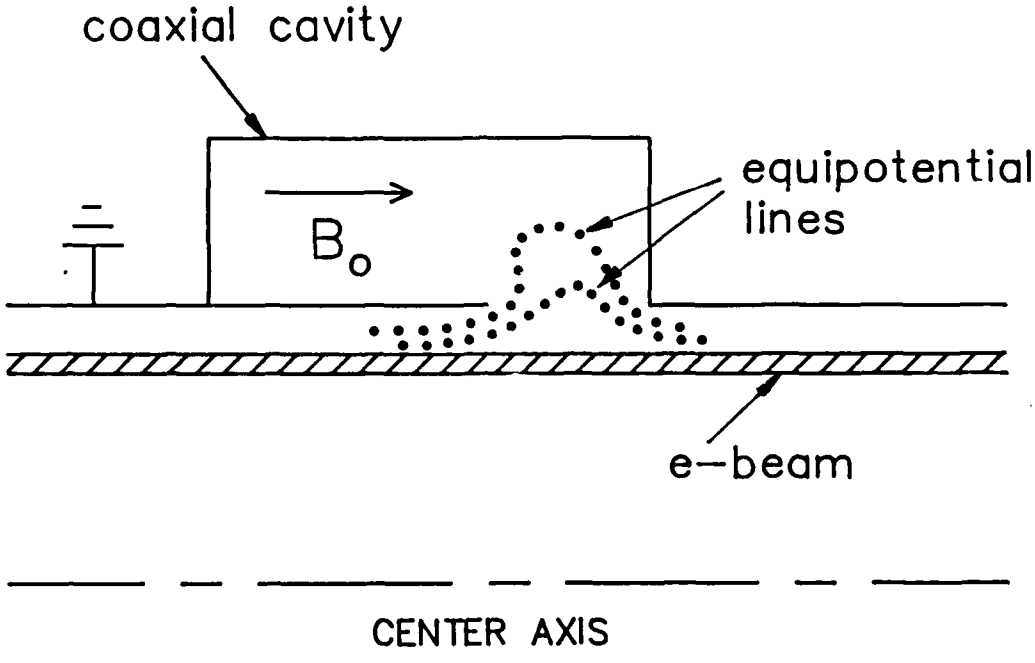

Fig. 4 Schematic drawings of the equipotential lines of the beam's self fields, which provide electrostatic insulation at the gap. The external magnetic field (B_o) provides magnetic insulation within the coaxial cavity.

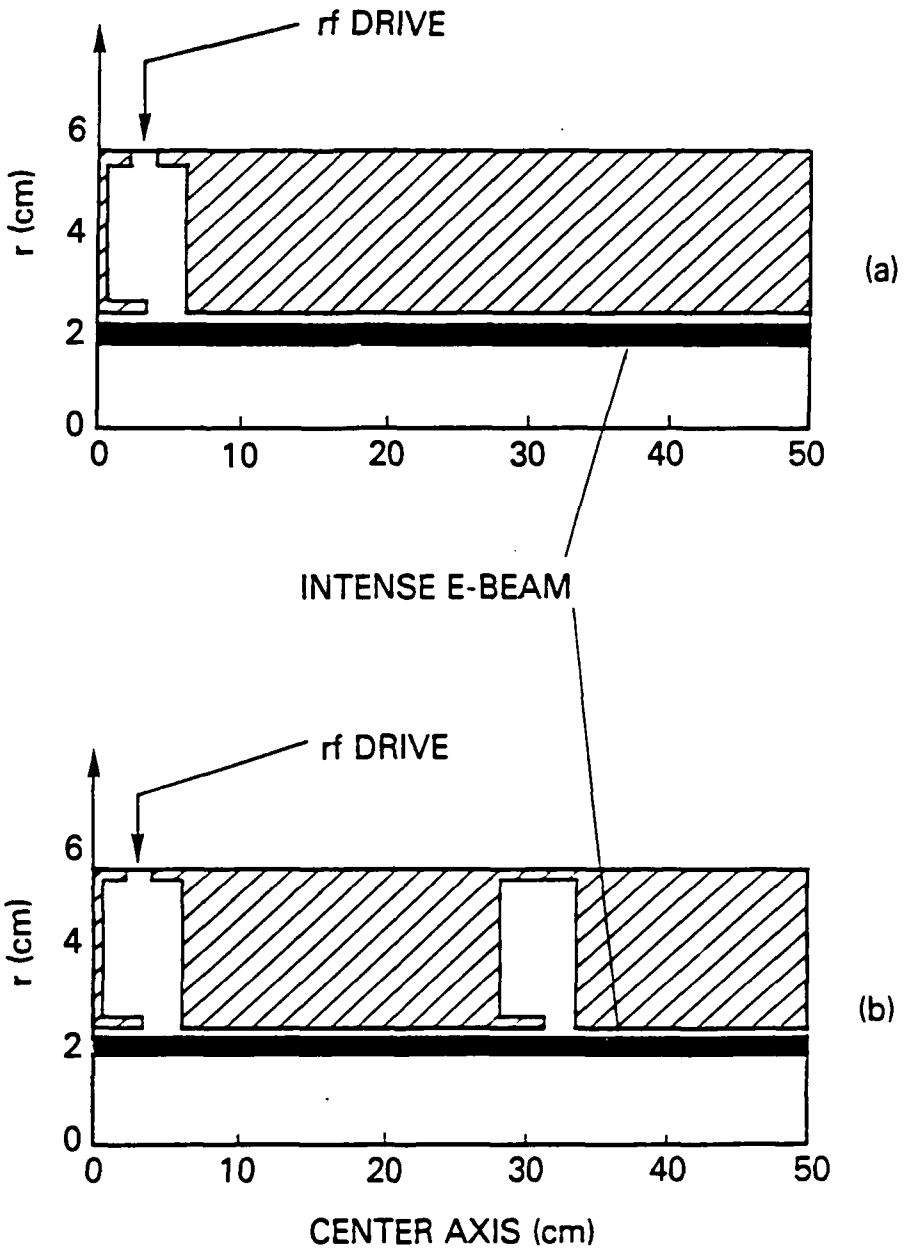

Fig. 5 The geometry used in simulating the small diameter beam. (a) Current modulation is provided by the externally driven cavity at left. (b) A second cavity is inserted to enhance current modulation.

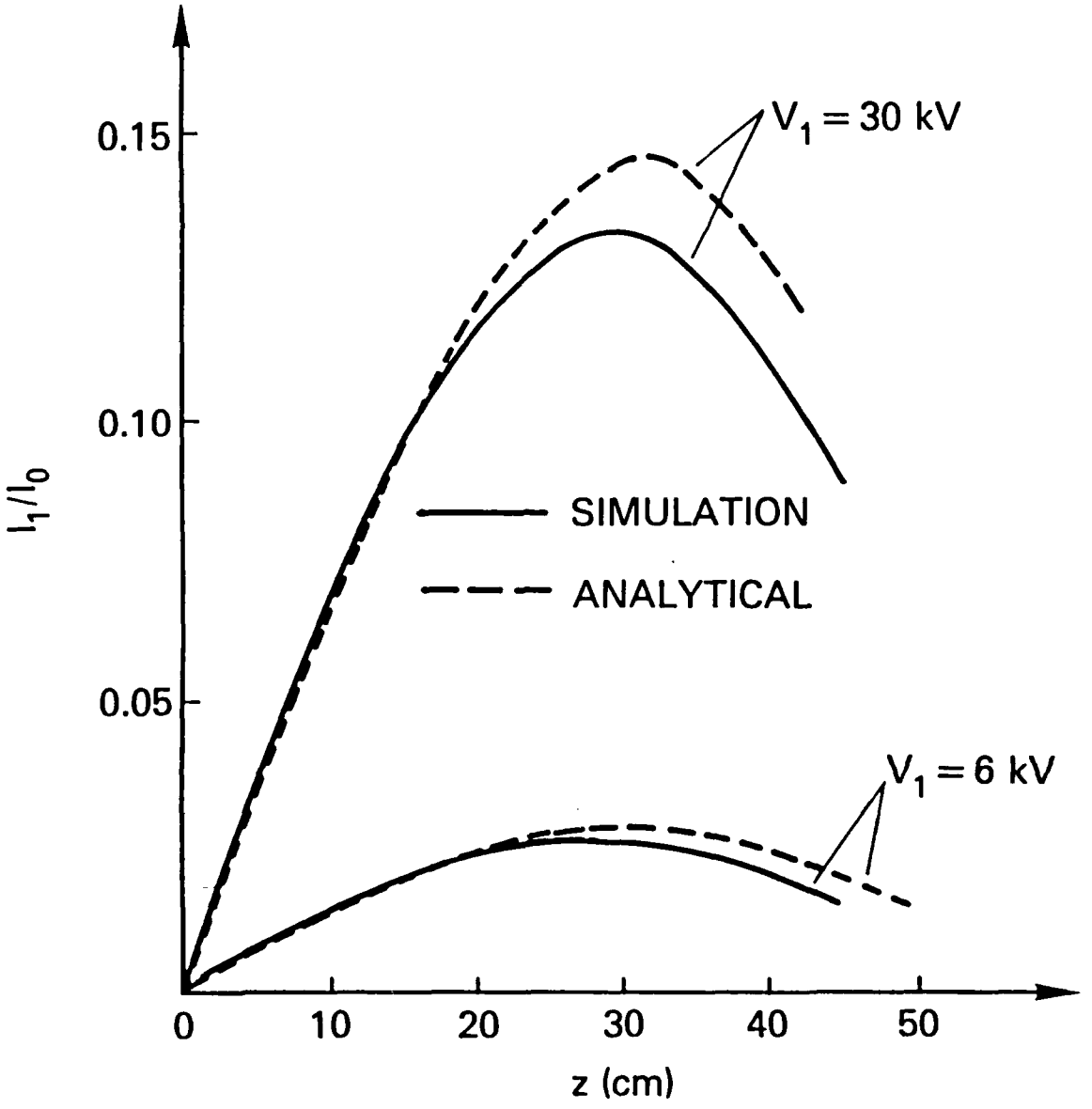

Fig. 6 Fraction of the modulated current for Fig. 5(a), at two levels of the rf drive. The dashed curve was obtained from the analytic formula, Eq. (9).

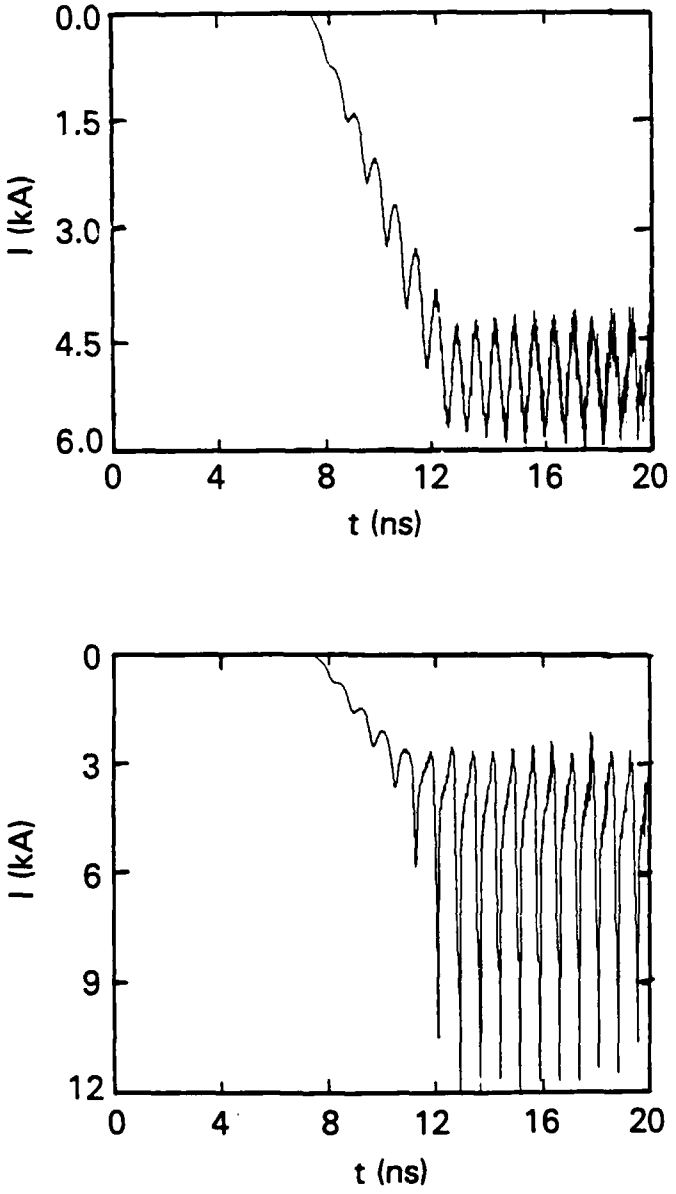

Fig. 7 (a) Current response measured at z = 28 cm from the gap for Fig. 5(a), with gap voltage V_1 = 30 kV. (b) Current response measured at 6 cm downstream of the second (right) cavity in Fig. 5(b), with V_1 = 30 kV at the first cavity.

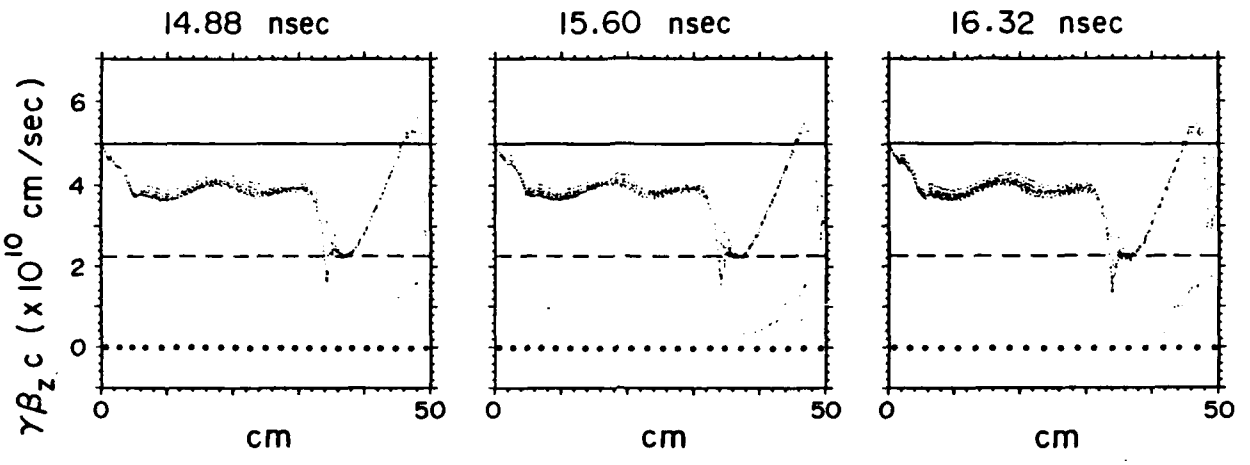

Fig. 8 Phase space plots for the two-cavity case at intervals of a cycle T = 0.73 ns. Solid lines show $\gamma\beta_z c$ at injection. Broken lines show $\gamma\beta_z c$ at a condition of dc limiting current ($\gamma = \gamma_{inj}^{1/3}$). Dotted lines show $\gamma\beta_z c = 0$. The geometry is shown in Fig. 5b.

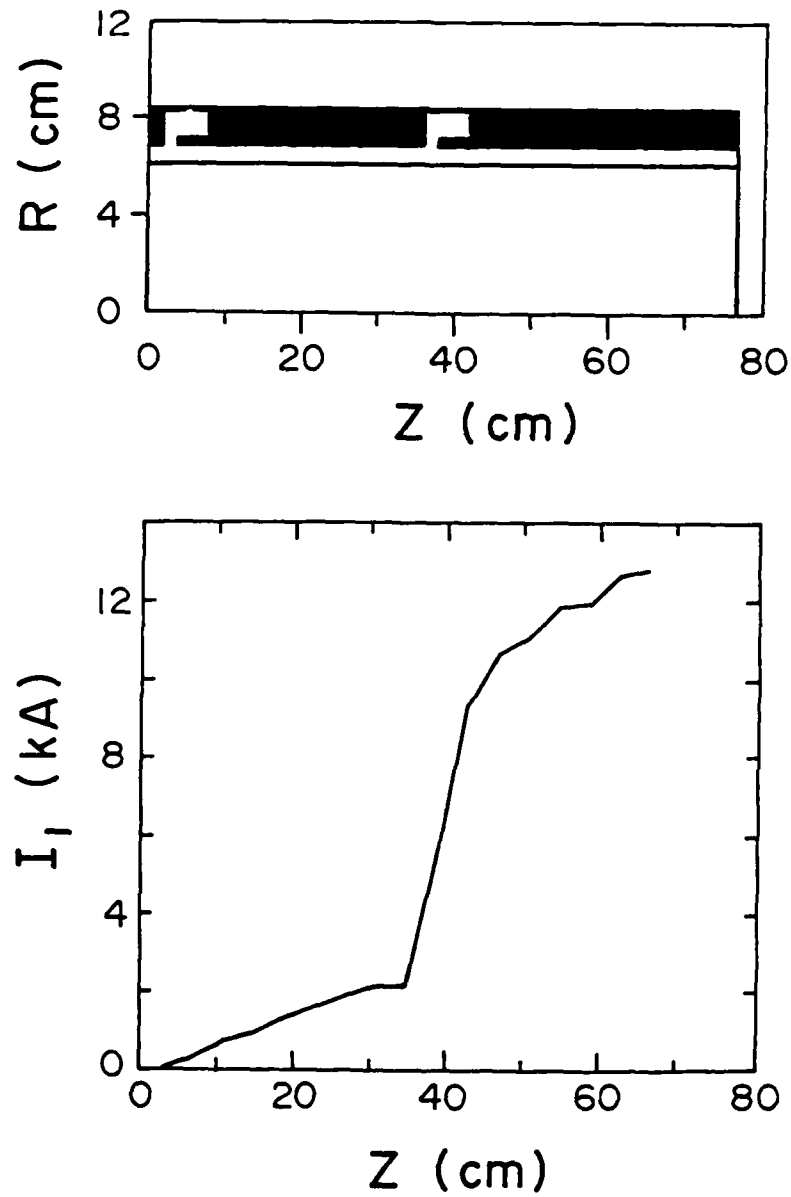

Fig. 9 The geometry used in simulating the large diameter beam (top) and the rf current modulation (bottom).

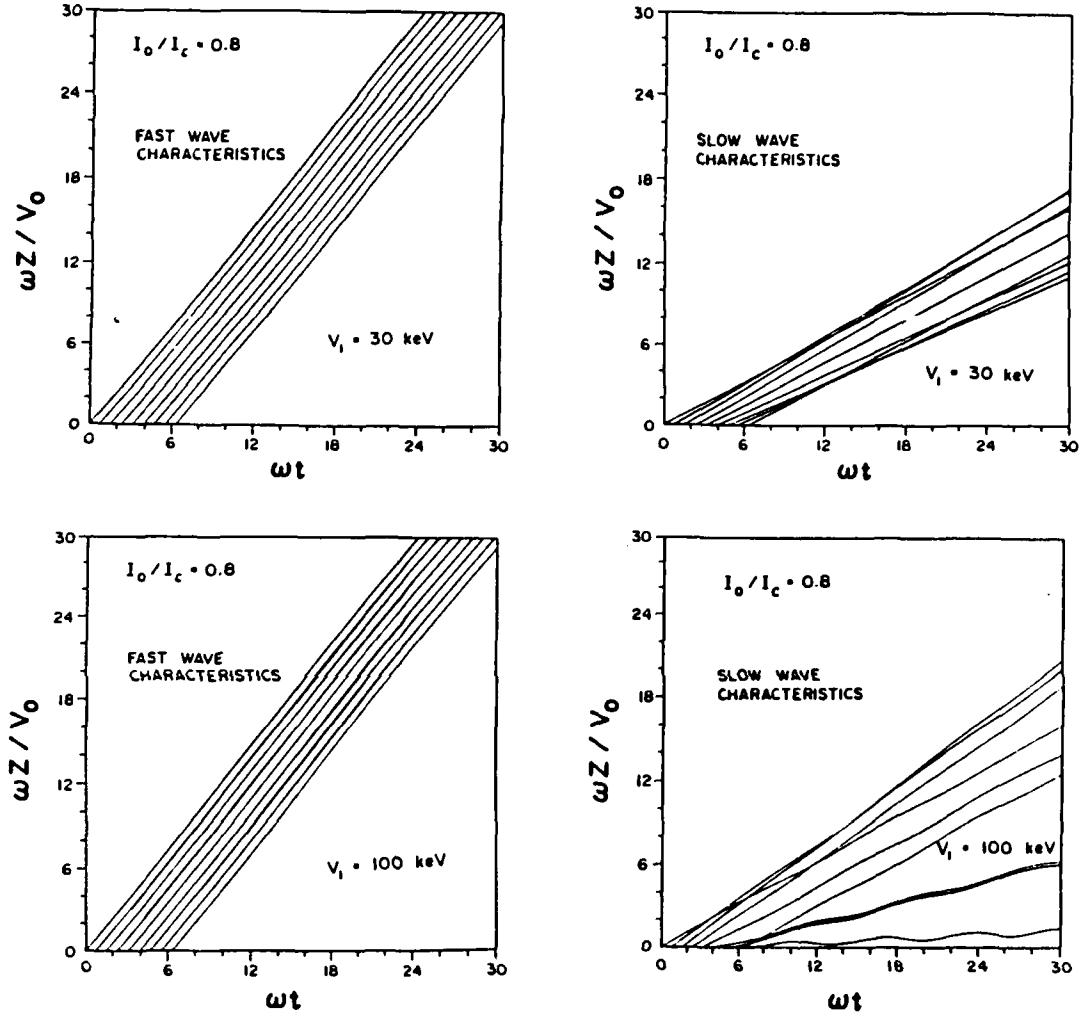

Fig. 10 The nonlinear propagation characteristics of the fast- and slow-waves on an IREB (E_{inj} = 425 keV, I_c = 12.8 kA) which is subject to a sinusoidal gap voltage V_1 at z = 0. The crossing of the slow-wave characteristics near z = 0 means strong current modulation near the gap exit, as a result of nonlinear and DC space charge effects.

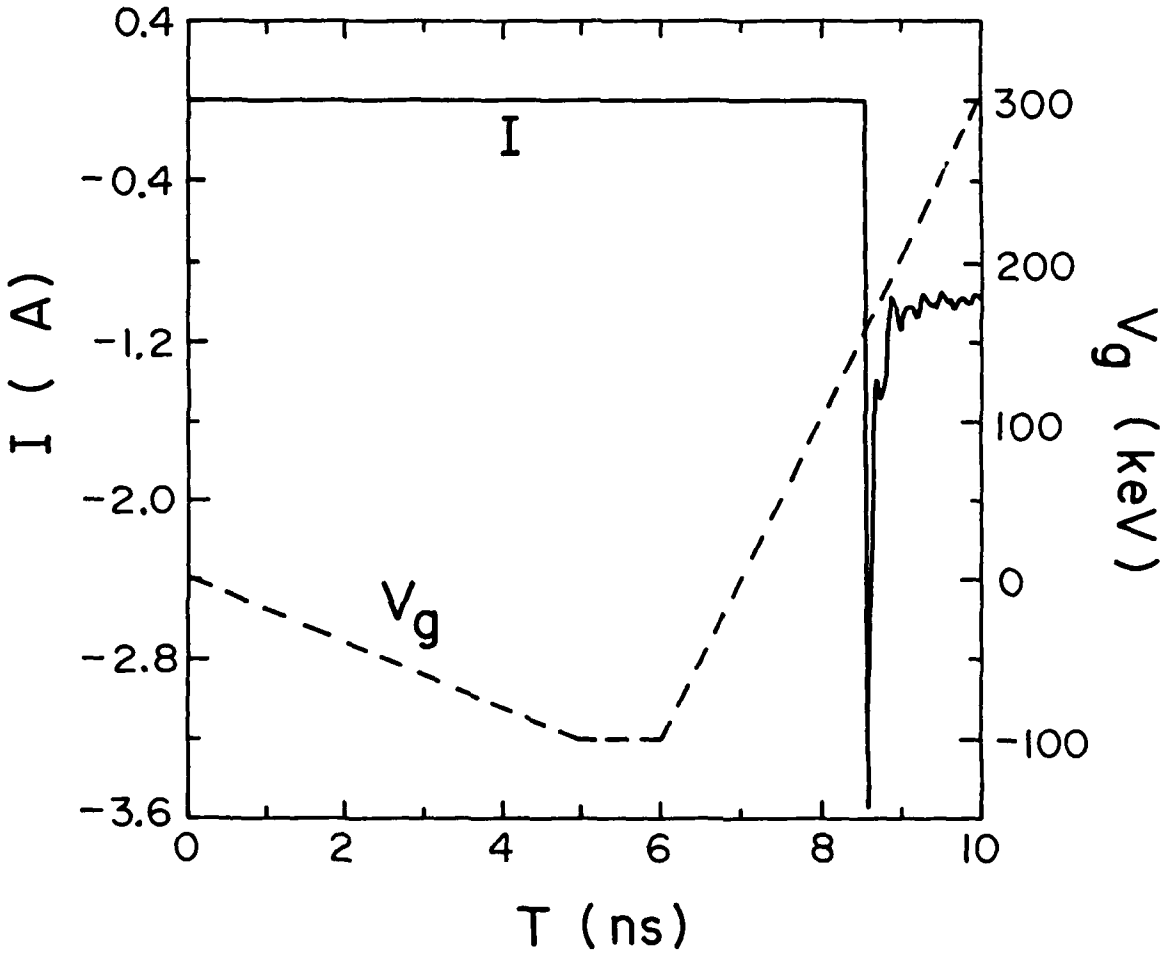

Fig. 11. Imposed gap voltage (V_g) and the leakage current (I) across the gap.

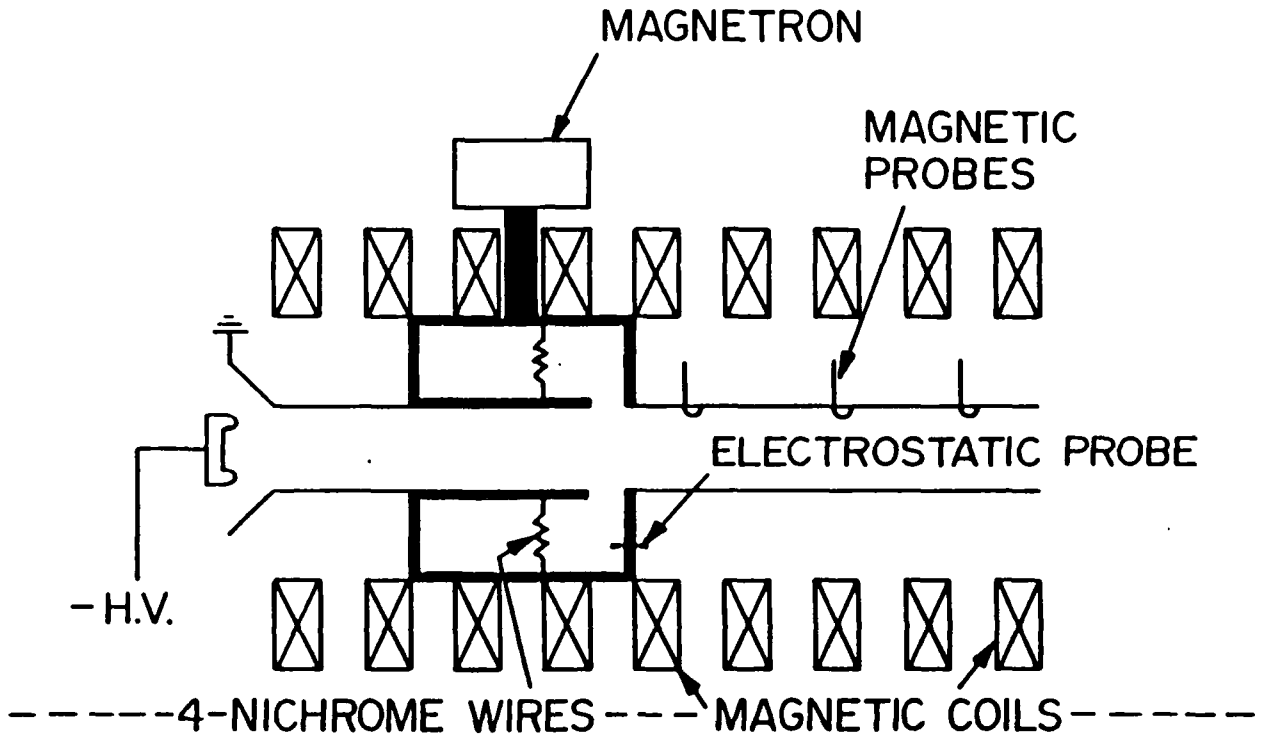

Fig. 12 Experimental arrangement when only one cavity was used.

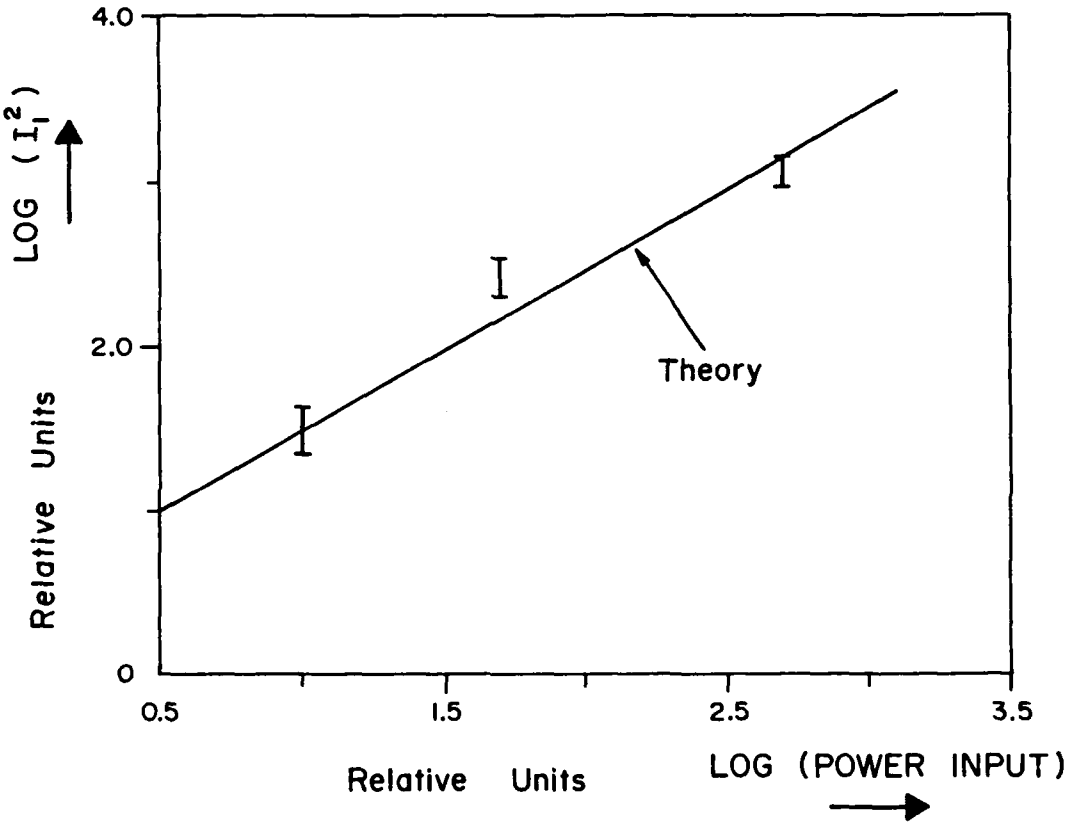

Fig. 13 Dependence of the IREB rf current on the input rf signal.

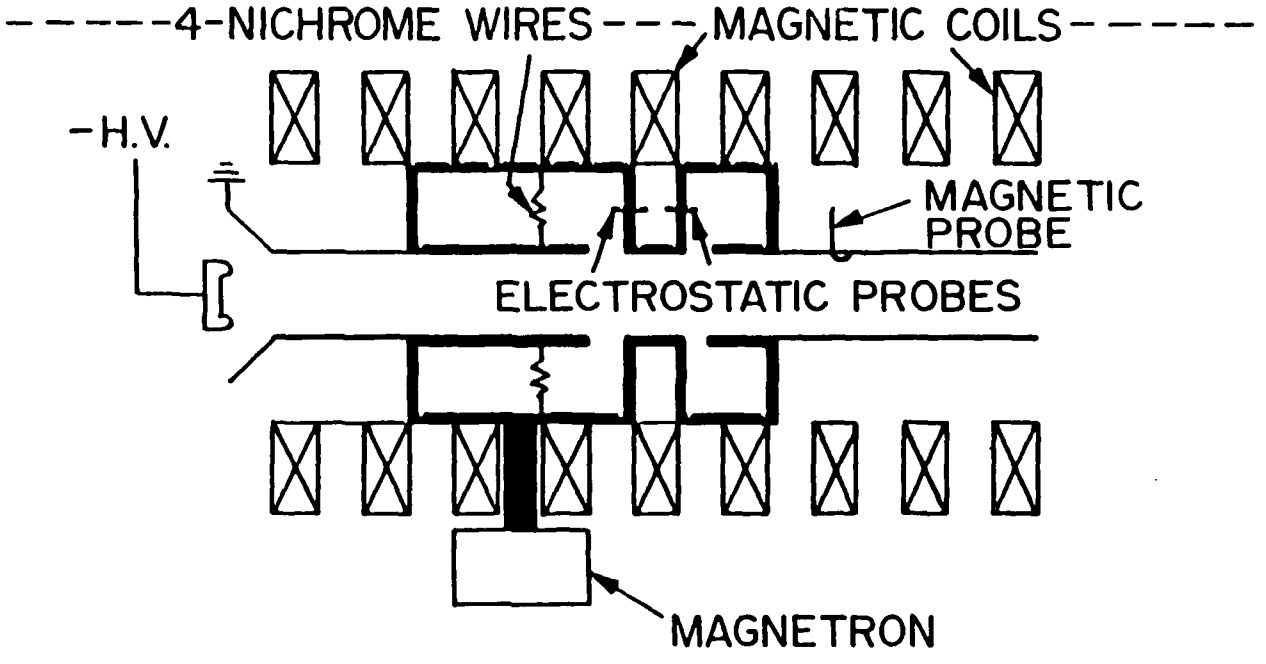

Fig. 14 Experimental arrangement when two cavities were used.

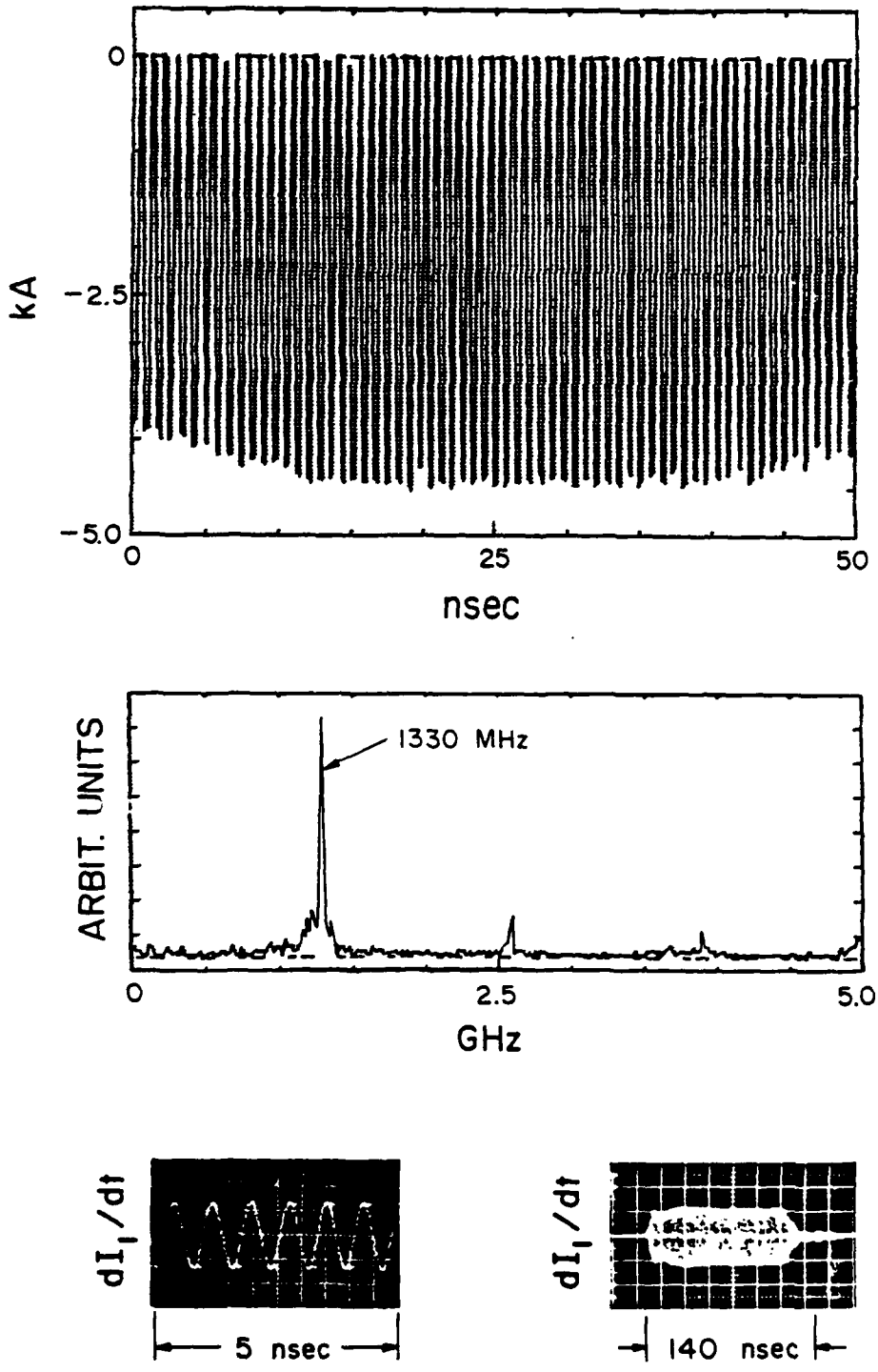

Fig. 15 Experimental results when the configuration of Fig. 13 was used. Top: rf current of the modulated IREB. Middle: Spectrum of dI/dt. Bottom: dI/dt traces obtained from 1 GHz Tektronix oscilloscope 7104.

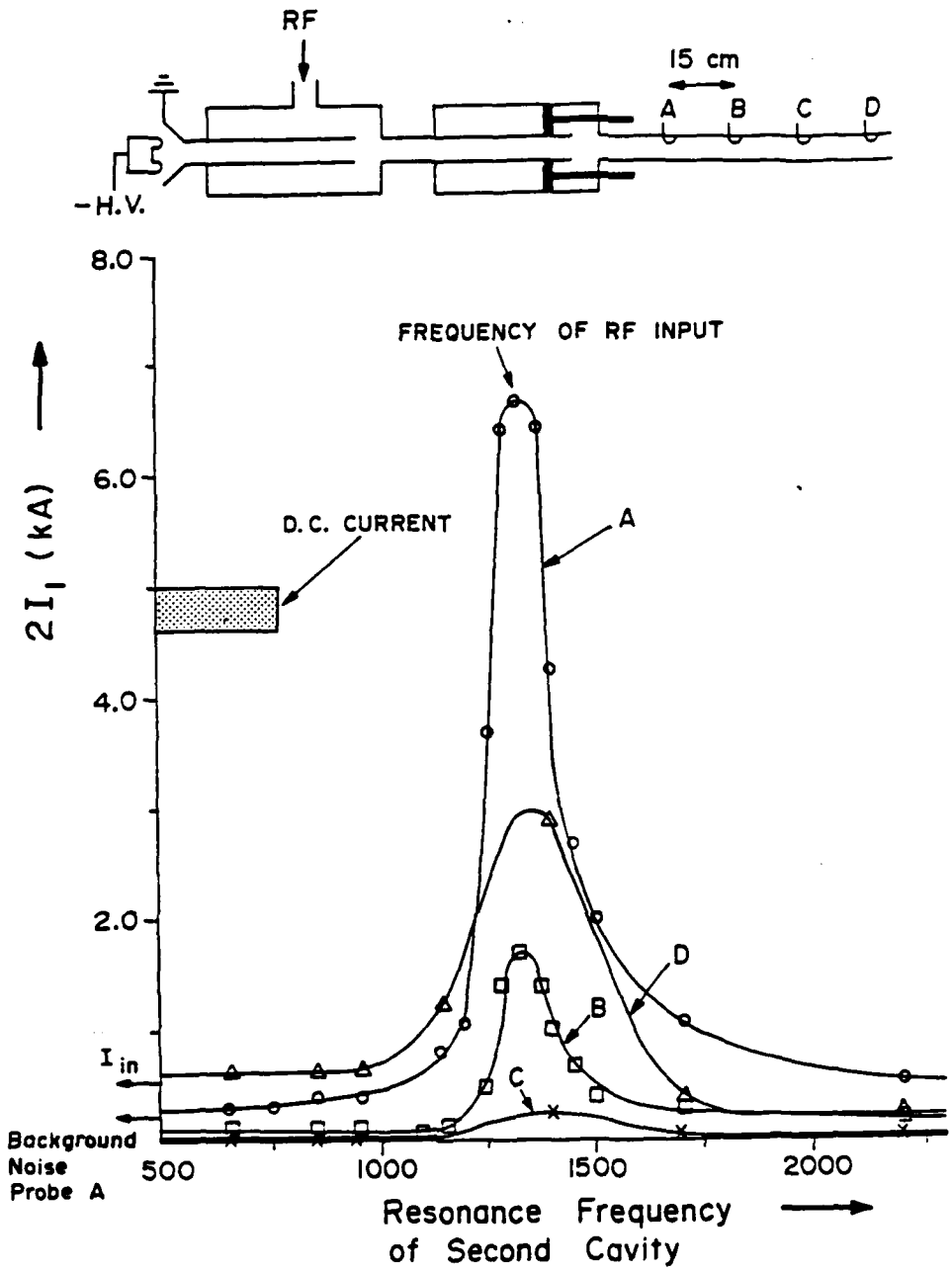

Fig. 16 (a) Top: Experimental arrangement. (b) Bottom: Peak bunch current as measured by the four magnetic probes. The shaded area represents the DC current. The arrow marked I_{in} is the level of the peak bunch current measured between the cavities. The arrow at the lower left corner shows the level of the background noise.

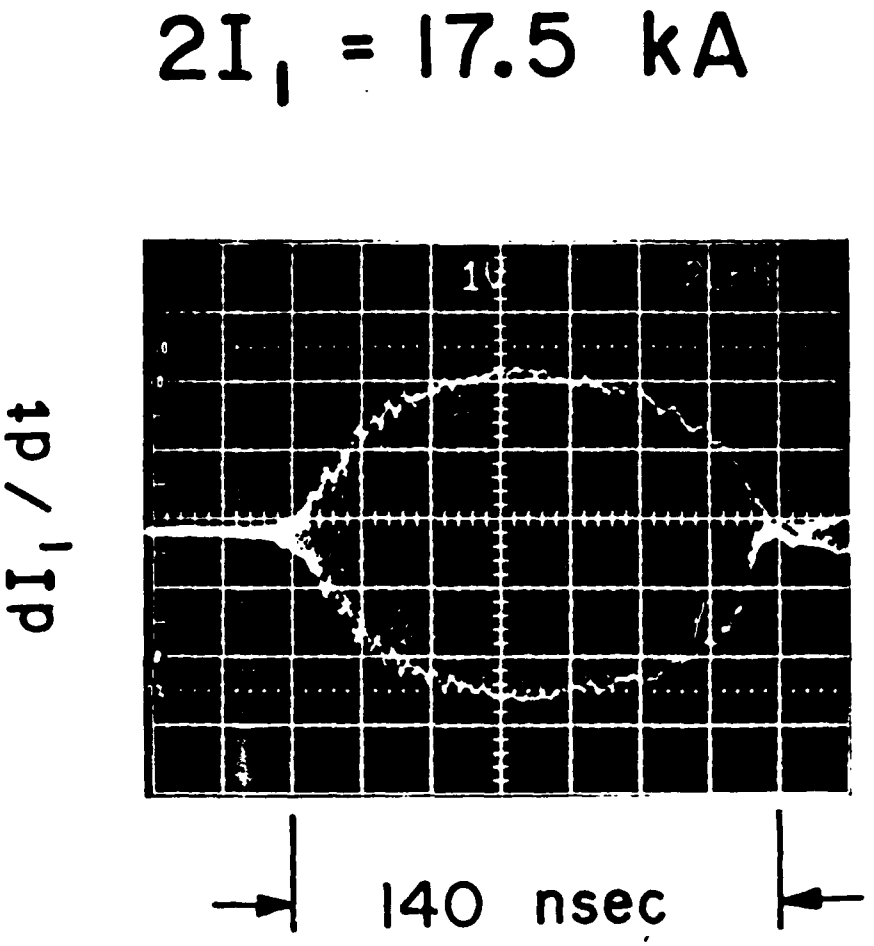

Fig. 17 Time derivative of the IREB current measured by the 1 GHz 7104 oscilloscope.

Equivalent Circuit for the RF Extraction System

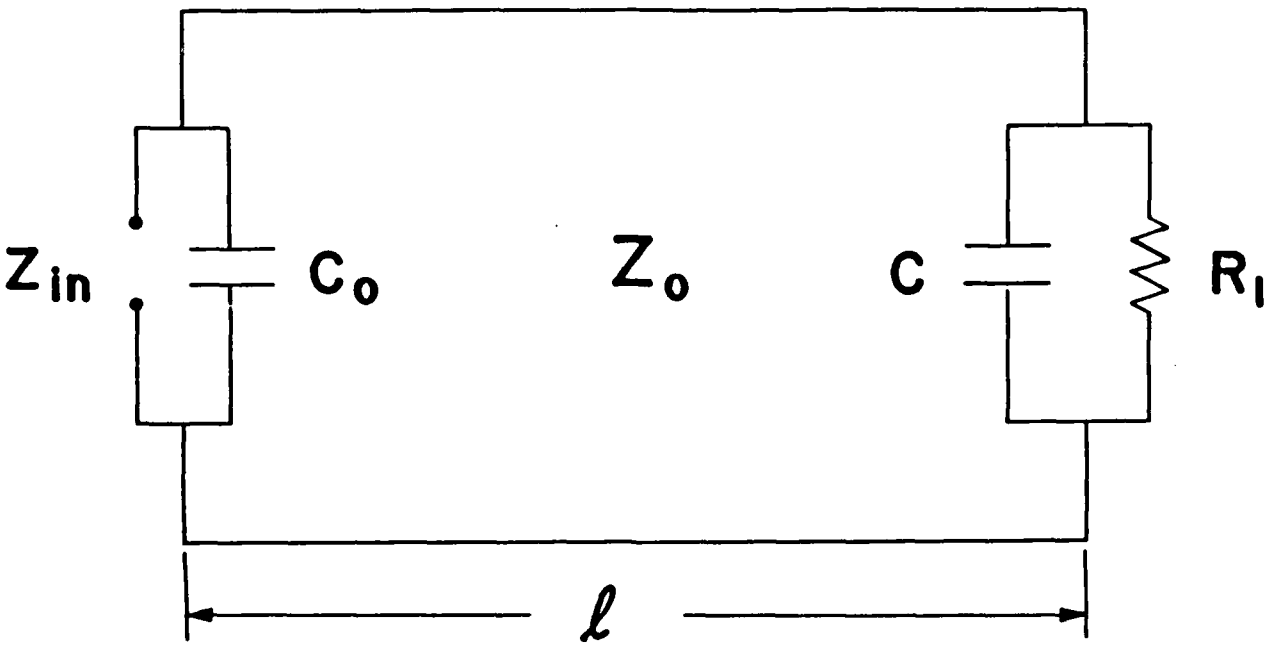

$$Z_{in} = R + jX$$

Fig. 18 Equivalent circuit of the RF convector.

Real and Imaginary Components of the Input Impedance Z_{in} vs Length

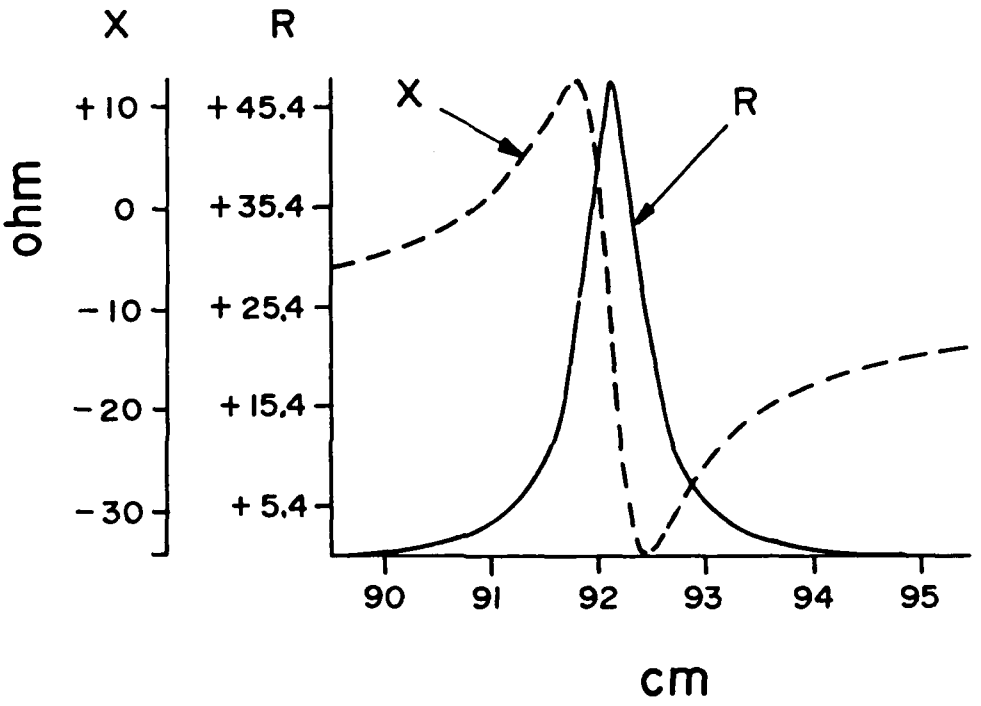

Fig. 19 Real and imaginary components of the input impedance Z_{in} vs length.

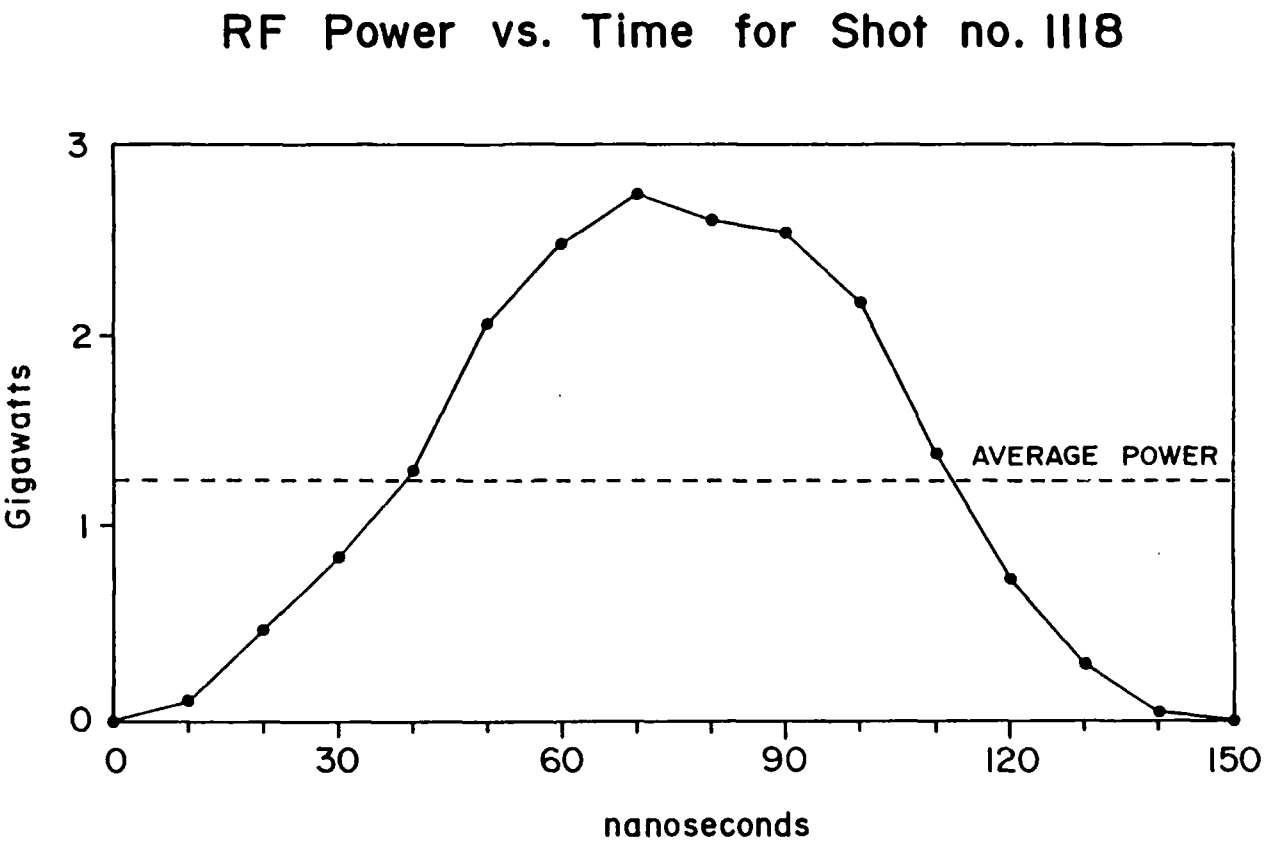

Fig. 20 Measured rf power vs time.

HIGH POWER MODE CONVERTER
FOR THE RELATIVISTIC
KLYSTRON AMPLIFIER

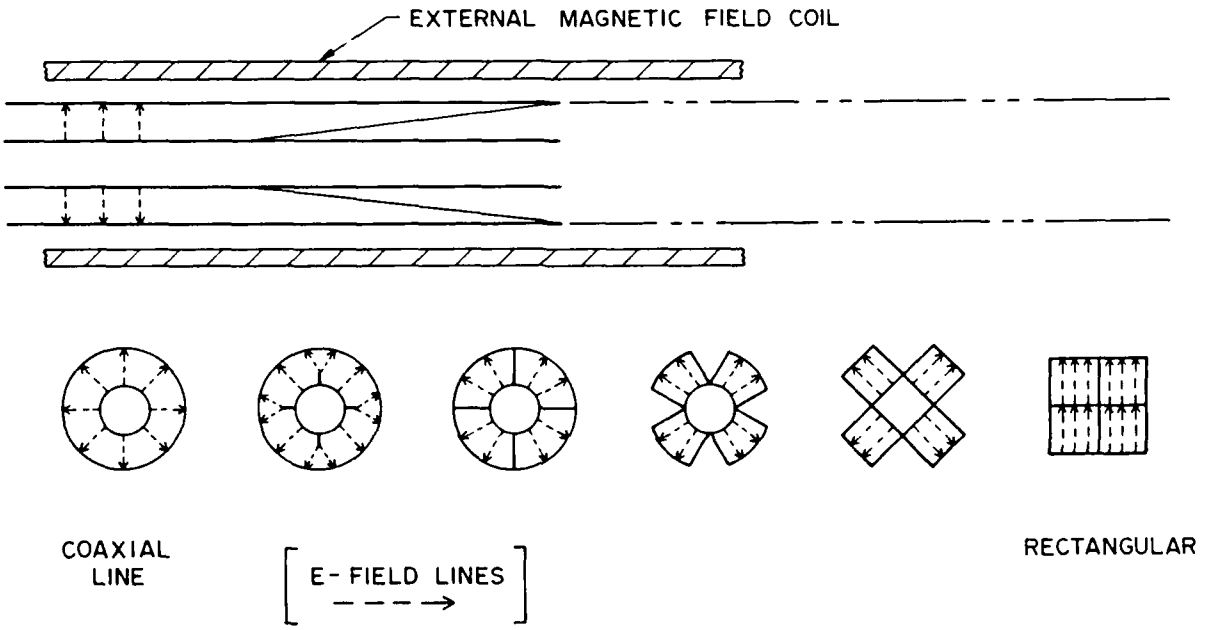

Fig. 21 High power mode converter.

DISTRIBUTION LIST*

Naval Research Laboratory
4555 Overlook Avenue, S.W.
Washington, DC 20375-5000

Attn: Code 1000 - Commanding Officer, CAPT J. J. Donegan, Jr.
1001 - Dr. T. Coffey
1005 - Head, Office of Management & Admin.
1005.1- Deputy Head, Office of Mgt & Admin.
1005.6 - Head, Directives Staff
1220 - Mr. M. Ferguson
2000 - Director of Technical Services
2604 - NRL Historian
2628 - Documents (22 copies)
2634 - D. Wilbanks
4000 - Dr. W. R. Ellis
4600 - Dr. D. Nagel
4603 - Dr. W. W. Zachary
4700 - Dr. S. Ossakow (26 copies)
4700.1 - Dr. M. Friedman (10 copies)
4700.1 - V. Serlin (10 copies)
4707 - Dr. W. M. Manheimer
4730 - Dr. S. Bodner
4780 - Dr. B. Ripin
4790 - Dr. P. Sprangle
4790 - Dr. Y. Y. Lau (40 copies)
4790 - Dr. D. G. Colombant
4790 - Dr. J. Krall (10 copies)
4790 - Dr. C. M. Tang
4790 - Dr. M. Lampe
4790 - Dr. G. Joyce
4790 - Dr. I. Haber
4790 - Dr. R. Hubbard
4790 - Dr. R. Fernsler
4790 - Dr. S. Slinker
4790 - Dr. T. Godlove
4790A- B. Pitcher
4793 - Dr. S. Gold
4795 - Dr. C. A. Kapetanakos
6840 - Dr. R. K. Parker
0124 - ONR

* Every name listed on distribution gets one copy except for those where extra copies are noted.

Prof. I. Alexeff
Dept. of Electrical Engineering
University of Tennessee
Knoxville, TN 37996-2100

Dr. Matthew A. Allen
Stanford Linear Accelerator Center
P. O. Box 4349, Bin 33
Stanford, CA 94309

Dr. T. Antonsen
University of Maryland
College Park, MD 20742

Assistant Secretary of the
Air Force (RD&L)
Room 4E856, The Pentagon
Washington, D.C. 20330

Dr. William L. Baker (2 copies)
Air Force Weapons Laboratory
Kirkland AFB
Albuquerque, NM 87117

Dr. W. A. Barletta
Lawrence Livermore National Lab.
P. O. Box 808
Livermore, CA 94550

Dr. L. R. Barnett
3053 Merrill Eng. Bldg.
University of Utah
Salt Lake City UT 84112

Dr. G. Bekefi
Mass. Institute of Tech.
Bldg. 26
Cambridge, MA 02139

Dr. Jim Benford
Physics International, Inc.
2700 Merced Street
San Leandro, CA 20301

Prof. Herbert Berk
Institute for Fusion Studies
University of Texas
Austin, TX 78712

Dr. I. B. Bernstein
Mason Laboratory
Yale University
400 Temple Street
New Haven, CT 06520

Prof. A. Bers
Dept. of Electrical Engineering
MIT
Cambridge, MA 02139

Prof. Charles K. Birdsall
Dept. of Electrical Engineering
University of California
Berkeley, CA 94720

Dr. H. Brandt (5 copies)
Harry Diamond Laboratory
SLCHD-NW-TN
2800 Powder Mill Rd.
Adelphi, MD 20783-1197

Dr. Charles Brau
Dept. of Physics & Astronomy
Vanderbilt University
Nashville, TN 37235

Dr. R. Briggs
SSC Laboratory, Suite 26
Stoneridge Office Park
2550 Beckleymeade Ave
Dallas, TX 75237

Dr. Edward A. Brown
Harry A. Diamond Laboratory
2800 Powder Mill Road
Adelphi, MD 20783-1197

Dr. Lee Buchanan
DARPA/DEO
1400 Wilson Blvd.
Arlington, VA 22209

Prof. O. Buneman
ERL, Stanford University
Stanford, CA 94305

Dr. K. J. Button
Francis Bitter Natl. Magnet Lab.
Mass. Institute of Technology
Cambridge, MA 02139

Prof. J. D. Callen
Nuclear Engineering Dept.
University of Wisconsin
Madison, WI 53706

Dr. Malcolm Caplan
Lawrence Livermore National Laboratory
P. O. Box 808
Livermore, CA 94550

Dr. Maria Caponi
TRW, Building R-1, Room 1184
One Space Park
Redondo Beach, CA 90278

Dr. George Caporaso
L-626
Lawrence Livermore National Laboratory
P. O. Box 808
Livermore, CA 94550

Prof. Frank Chan
School of Eng. & Applied Sciences
Univ. of Calif. at Los Angeles
7731 K Boelter Hall
Los Angeles, CA 90024

Dr. V. S. Chan
GA Technologies
P.O. Box 85608
San Diego, CA 92138

Dr. D. P. Chernin
Science Applications Intl. Corp.
1720 Goodridge Drive
McLean, VA 22102

Prof. M. V. Chodorow
Ginzton Laboratory
Stanford, University
Stanford, CA 94305

Dr. William Colson
Berkeley Research Asso.
P. O. Box 241
Berkeley, CA 94701

Dr. Richard Cooper
Los Alamos National Scientific
Laboratory
P.O. Box 1663
Los Alamos, NM 87545

Dr. Bruce Danly
MIT
NW16-174
Cambridge, MA 02139

Dr. R. Davidson
Plasma Fusion Center
Mass. Institute of Tech.
Cambridge, MA 02139

Dr. John Dawson
Physics Department
University of California
Los Angeles, CA 90024

Dr. David A. G. Deacon
Deacon Research
2440 Embarcadero Way
Palo Alto, CA 94303

Deputy Under Secretary of
Defense for R&AT
Room 3E114, The Pentagon
Washington, D.C. 20301

Dr. W. W. Destler
Dept. of Electrical Engineering
University of Maryland
College Park, MD 20742

Director of Research (2 copies)
U. S. Naval Academy
Annapolis, MD 21402

Dr. Gunter Dohler
Northrop Corporation
Defense Systems Division
600 Hicks Road
Rolling Meadows, IL 60008

Dr. A. Drobot
Science Applications Intl. Corp.
1710 Goodridge Road
McLean, VA 22102

Dr. Dwight Duston
Strategic Defense Initiative Org.
OSD/SDIO/IST
Washington, DC 20301-7100

Dr. Luis R. Elias
Quantum Institute
University of California
Santa Barbara, CA 93106

Dr. Kenneth Eppley
Stanford Linear Accelerator Center
P. O. Box 4349, Bin 26
Stanford, CA 94309

Dr. W. Fawley
L-626
Lawrence Livermore National Laboratory
P. O. Box 808
Livermore, CA 94550

Dr. H. Fleischmann
Cornell University
Ithaca, NY 14850

Dr. Wei Gai
Argonne National Laboratory
9700 S. Cass Avenue
Argonne, IL 60439

Dr. R. Gajewski
Div. of Advanced Energy Projects
U. S. Dept of Energy
Washington, DC 20545

Prof. Ward Getty
University of Michigan
Ann Arbor, MI 48109

Prof. Ronald Gilgenbach
Dept. Nucl. Engineering
University of Michigan
Ann Arbor, MI 48109

Dr. R. L. Gluckstern
Physics Department
University of Maryland
College Park, MD 20742

Dr. B. B. Godfrey,
Chief Scientist
WL/CA
Kirtland AFB. NM 87117-6008

Dr. V. L. Granatstein
Dept. of Electrical Engineering
University of Maryland
College Park, MD 20742

Prof. Herman A. Haus
Mass. Institute of Technology
Rm. 36-351
Cambridge, MA 02139

Dr. Richard Helm
Stanford Linear Accelerator Center
P. O. Box 4349, Bin 26
Stanford, CA 94309

Dr. William Herrmannsfeldt
Stanford Linear Accelerator Center
P. O. Box 4349
Stanford, CA 94305

Dr. Donald B. Hopkins
Lawrence Berkeley Laboratory
One Cyclotron Road
Berkeley, CA 94720

Dr. Bertram Hui
DARPA
1400 Wilson Blvd.
Arlington, VA 22209

Dr. Stanley Humphries, Jr.
Dept. Chemical & Nuclear Engineering
University of New Mexico
Albuquerque, NM 87131

Dr. J. Jacob
Science Research Laboratory
15 Ward Street
Sommerville, MA 02143

Dr. G. L. Johnston
NW 16-232
Mass. Institute of Tech.
Cambridge, MA 02139

Dr. Howard Jory
Varian Associates, Bldg. 1
611 Hansen Way
Palo Alto, CA 94303

Prof. Terry Kammash
University of Michigan
Ann Arbor, MI 48109

Prof. Donald Kerst
3291 Chamberlin Hall
University of Wisconsin
Madison, WI 53706

Dr. K. J. Kim, MS-101
Lawrence Berkeley Lab.
Rm. 223, B-80
Berkeley, CA 94720

Prof. N. M. Kroll
Department of Physics
B-019, UCSD
La Jolla, CA 92093

Dr. Thomas Kwan
Los Alamos National Scientific
Laboratory, MS608
P. O. Box 1663
Los Alamos, NM 87545

Dr. Theodore L. Lavine
Stanford Linear Accelerator Center
P. O. Box 4349, Bin 26
Stanford, CA 94309

Dr. Edward P. Lee
Lawrence Berkeley Laboratory
1 Cyclotron Road
Berkeley, CA 94720

Dr. Terry G. Lee
Stanford Linear Accelerator Center
P. O. box 4349, Bin 30
Stanford, CA 94309

Dr. Rulon K. Linford
CTR-11, Mail Stop: 646
Los Alamos National Laboratory
P. O. Box 1663
Los Alamos, NM 87545

Dr. Gregory A. Loew
Stanford Linear Accelerator Center
P. O. Box 4349, Bin 33
Stanford, CA 94309

Prof. J. M. J. Madey
117 Physics Bldg.
Duke University
Durham, NC 27706

Dr. J. A. Mangano
Science Research Laboratory
15 Ward Street
Sommerville, MA 02143

Dr. J. Mark
Lawrence Livermore National Lab.
Attn: L-477
P. O. Box 808
Livermore, CA 94550

Dr. Roger Miller
Stanford Linear Accelerator Center
P. O. Box 4349, Bin 26
Stanford, CA 94309

Dr. A. Mondelli
Science Applications Intl. Corp.
1710 Goodridge Drive
McLean, VA 22102

Prof. George Morales
Dept. of Physics
U.C.L.A.
Los Angeles, CA 90024

Dr. Philip Morton
BIN26
Stanford Linear Accelerator Center
P.O. Box 4349
Stanford, CA 94305

Dr. J. Nation
Cornell University
Ithaca, NY 14850

Dr. Kelvin Neil
Lawrence Livermore National Lab.
Code L-321, P.O. Box 808
Livermore, CA 94550

Dr. T. Orzechowski
L-436
Lawrence Livermore National Lab.
P. O. Box 808
Livermore, CA 94550

Prof. E. Ott
Department of Physics
University of Maryland
College Park, MD 20742

Dr. Robert B. Palmer
Brookhaven National Laboratories
Associated Universities, Inc.
Upton, L.I., NY 11973

Dr. W. K. H. Panofsky
Stanford Linear Accelerator Center
P. O. Box 4349
Stanford, CA 94305

Dr. Richard H. Pantell
Stanford University
Stanford, CA 94305

Dr. R. R. Parker
NW16-288
Plasma Fusion Center
MIT
Cambridge, MA 02139

Dr. James M. Paterson
Stanford Linear Accelerator Center
P. O. Box 4349, Bin 26
Stanford, CA 94309

Dr. Claudio Pellegrini
Brookhaven National Laboratory
Associated Universities, Inc.
Upton, L.I., NY 11973

Dr. Sam Penner
National Bureau of Standards,
RADP B102
Washington, DC 20234

Dr. Jerry Peters
Office of High Ener. & Nuc. Physics
U. S. Dept. of Energy, GTN
Washington, DC 20545

Dr. Hersch Pilloff
Code 1112
Office of Naval Research
Arlington, VA 22217

Dr. Donald Prosnitz
Lawrence Livermore National Lab.
Attn: L-470
P. O. Box 808
Livermore, CA 94550

Dr. Sidney Putnam
Pulse Sciences, Inc.
600 McCormack Street
San Leandro, CA 94577

Dr. M. Reiser
University of Maryland
Department of Physics
College Park, MD 20742

Dr. Burton Richter
Stanford Linear Accelerator Center
P. O. Box 4349, Bin 80
Stanford, CA 94309

Dr. C. W. Roberson
Code 1112
Office of Naval Research
800 N. Quincy Street
Arlington, VA 22217

Dr. Marshall N. Rosenbluth
Physics Dept.
University of California, San Diego
La Jolla, CA 92093

Dr. James Rosenzweig
Fermi National Accelerator Center
Batavia, IL 60510

Dr. N. Rostoker
University of California
Department of Physics
Irvine, CA 92717

Dr. Ronald D. Ruth
Stanford Linear Accelerator Center
P. O. Box 4349, Bin 26
Stanford, CA 94309

Dr. E. T. Scharlesmann
L626
Lawrence Livermore National Laboratory
P. O. Box 808
Livermore, CA 94550

Dr. Michael Schlesinger
ONR Code 1112
800 N. Quincy Street
Arlington, VA 22217-5000

Dr. Howard Schlossberg
AFOSR
Bolling AFB
Washington, D.C. 20332

Dr. H. Schwettmann
Phys. Dept. & High Energy
Physics Laboratory
Stanford University
Stanford, CA 94305

Dr. A. M. Sessler
Lawrence Berkeley Laboratroy
University of California
1 Cyclotron Road
Berkeley, CA 94720

Dr. R. Shefer
Science Research Laboratory
15 Ward Street
Somerville, MA 02143

Dr. Charles Sinclair
C.E.B.A.F.
12000 Jefferson Avenue
Newport News, VA 23606

Dr. Lloyd Smith
Lawrence Berkeley Laboratory
University of California
1 Cyclotron Road
Berkeley, CA 94720

Dr. R. Sudan
Cornell University
Ithaca, NY 14850

Dr. David F. Sutter
ER 224, GTN
Department of Energy
Washington, D.C. 20545

Dr. T. Tajima
IFS
Univ. of Texas
Austin, TX 78712

Dr. R. Temkin
Mass. Institute of Technology
Plasma Fusion Center
Cambridge, MA 02139

Dr. Keith Thomassen, L-637
Lawrence Livermore National Laboratory
P. O. Box 808
Livermore, CA 94550

Dr. H. S. Uhm
Naval Surface Warfare Center
White Oak Lab.
Silver Spring, MD 20903

Under Secretary of Defense (R&E)
Office of the Secretary of Defense
Room 3E1006, The Pentagon
Washington, D.C. 20301

Dr. J. Walsh
Physics Department
Dartmouth College
Hanover, NH 03755

Dr. G. A. Westenskow
L-626
Lawrence Livermore National
P.O. Box 808
Livermore, CA 94550

Ms. Bettie Wilcox
Lawrence Livermore National Lab.
ATTN: Tech. Info. Dept. L-3
P.O. Box 808
Livermore, CA 94550

Dr. Perry Wilson
Stanford Linear Accelerator Center
P. O. Box 4349
Stanford, CA 94305

Dr. J. Wurtele
M.I.T.
NW 16-234
Plasma Fusion Center
Cambridge, MA 02139

Dr. David Yu
Duly Consultants
1912 MacArthur Street
Rancho Palo Verdes, CA 90732

Dr. S. S. Yu
L-626
Lawrence Livermore National Laboratory
P. O. Box 808
Livermore, CA 94550

Naval Research Laboratory
Washington, DC 20375-5000
Code 4830
Tim Calderwood

Director of Research
U.S. Naval Academy
Annapolis, MD 21402
(2 copies) 1-0

RECORDS - 1 copy